

An internal sensory model allows for balance control based on non-actionable proprioceptive feedback

Eric Maris*, #

**Donders Institute for Brain, Cognition, and Behaviour, Radboud University, P.O. Box 9104 HE Nijmegen*

#

Corresponding Author:

Eric Maris

e-mail: e.maris@donders.ru.nl

tel: +31243612651

The total number of words of the manuscript, including entire text from title page to figure legends: **10990**

The number of words of the abstract: **181**

The number of figures: **4**

The number of tables: **0**

Abstract

All motor tasks with a mechanical system (a human body, a rider on a bicycle) that is approximately linear in the part of the state space where it stays most of the time (e.g., upright balance control) have the following property: actionable sensory feedback allows for optimal control actions that are a simple linear combination of the sensory feedback. When only non-actionable sensory feedback is available, optimal control for these approximately linear mechanical systems is based on an internal dynamical system that estimates the states, and that can be implemented as a recurrent neural network (RNN). It uses a sensory model to update the state estimates with the non-actionable sensory feedback, and the weights of this RNN are fully specified by results from optimal feedback control. This is highly relevant for muscle spindle afferent firing rates which, under perfectly coordinated fusimotor and skeletomotor control, scale with the exafferent joint acceleration component. The resulting control mechanism balances a standing body and a rider-bicycle combination using realistic parameter values and with forcing torques that are feasible for humans.

Keywords

Internal model, sensory model, recurrent neural network, balance control, standing balance, bicycle balance, muscle spindles, fusimotor control, exafferent sensory feedback, closed-loop feedback control, optimal feedback control, linear quadratic Gaussian, underactuated.

Introduction

Most of our movements are goal-directed, and to achieve these goals our central nervous system (CNS) almost always requires sensory feedback. For example, staying upright while standing (standing balance control) depends on control actions in the form of ankle torques that overcome the toppling torque due to gravity and prevent the body from falling. These control actions are computed by the CNS and depend on sensory feedback about the body's center of gravity (CoG) relative to its area of support (AoS). The situation is similar in other forms of balance control, such as on the bicycle: the control actions now involve steering (turning the handlebars), and the sensory feedback pertains to the combined CoG of rider and bicycle relative to the line of support (LoS) that is formed by the two contact points between the tires and the road surface.

The difficulty of the CNS's control task depends on the sensory feedback. This can be demonstrated rigorously for the case of the CNS controlling a linear mechanical system. This mechanical system consists of the body's musculo-skeletal system plus the objects that are attached to it (e.g., a bicycle, a cane, a pencil). The mechanical system is linear if the limb movements are described by a set of differential equations that are linear in the limbs' positions and velocities, the system's state variables. For several motor tasks, such as balance control, the mechanical system is linear near the so-called fixed point, and for a standing body and a rider-bicycle combination, this is the upright position. In balance control, because the fixed point is above the AoS/LoS, most of the movements remain close to it. This is the situation that we will consider in this paper. For a linear mechanical system, the optimal control action is a simple linear combination of the state variables [1]. Therefore, the control task for the CNS is easy if the sensory feedback is an accurate estimate of the

limbs' positions and velocities (the state variables); the optimal control action then is a simple linear combination of this sensory feedback. This type of sensory feedback will be called actionable.

The nature of the sensory feedback depends on the sensory organs. For balance control, the contributions of somatosensory (including proprioceptive), vestibular, visual and auditory feedback have all been investigated [2]. I will focus on proprioceptive feedback from the muscle spindles [3]. There is good empirical evidence that, at least on a firm and immobile support surface, this proprioceptive feedback is sufficient for standing balance control [4-6]. However, I will argue that it is not actionable because the muscle spindles do not provide direct information about joint angular position and velocity [7-10]. This raises the question how the CNS can use proprioceptive feedback to keep the body upright. I will demonstrate that this is possible by making use of a CNS-internal sensory model of the proprioceptive feedback. Crucially, this sensory model agrees with results from sensory neurophysiology. Specifically, these results are consistent with the view that, under perfectly coordinated skeletomotor and fusimotor control, muscle spindle afferent firing rates scale with the exafferent joint acceleration component. This sensory model can be combined with the familiar internal model for the dynamics of the mechanical system [11, 12], and together they specify a dynamical system that estimates the current state. This CNS-internal dynamical system can be implemented as a recurrent neural network (RNN).

The evidence in the present paper comes from formal analysis and computer simulations, and the main point can be made convincingly using the one degree-of-freedom (1-DoF) inverted pendulum model of standing balance control. Focusing on such a simple model has the risk of making general claims about motor control that are only valid for this simple

model system. I will mitigate this risk by making the same point using two 3-DoF models for bicycle balance control. Balancing a bicycle using only proprioceptive feedback is a very challenging control problem because the mechanical system is underactuated [13]: because the rider is not touching the road surface, the bicycle lean angle cannot be controlled by a forcing torque over the roll axis. I will demonstrate that a bicycle can be balanced using only non-actionable proprioceptive feedback from the rider's upper body and a steering torque that controls the front frame via the handlebars.

Results

A closed-loop feedback control model for standing balance

In Fig. 1A and 1B, a closed-loop feedback control model is shown [14-16]. In its application to standing balance control, the mechanical system (in red) is the body's musculo-skeletal system, which is depicted separately in Fig. 1C. This mechanical system is modeled as a compound inverted pendulum (CIP) that rotates about the ankle joint. The pendulum's angular position relative to gravity (lean angle) is denoted by θ and the muscular forcing torque at the ankle joint by \mathbf{z} . The movements of the CIP are fully specified by its equation of motion (EoM), which expresses the acceleration $\ddot{\theta}$ as a function of position θ , velocity $\dot{\theta}$, and the forcing torque z (see Eq. 3). The EoM is usually written as a function of the mechanical system's state, which is the combined position θ and velocity $\dot{\theta}$, and is denoted by $\mathbf{x} = [\theta, \dot{\theta}]^t$. The distinction between the state \mathbf{x} and the acceleration $\ddot{\theta}$ is crucial for balance control because the muscular forcing torque \mathbf{z} controls $\ddot{\theta}$ in a direct way, whereas the state variables θ and $\dot{\theta}$ are only controlled indirectly via $\ddot{\theta}$. The EoM can be written as a differential equation for the state \mathbf{x} , which I will denote as $\dot{\mathbf{x}} = \Phi(\mathbf{x}, \mathbf{z})$. This differential equation is usually called the EoM in state-space form, and it is described in more detail in *An optimal computational system for a linear approximation of the mechanical system*. (Here and in the following, I will not follow the notational convention of using lower case boldface letters for vectors and normal font for scalars; all results in this paper hold for the vector-valued case, but sometimes the application/example involves only scalars.)

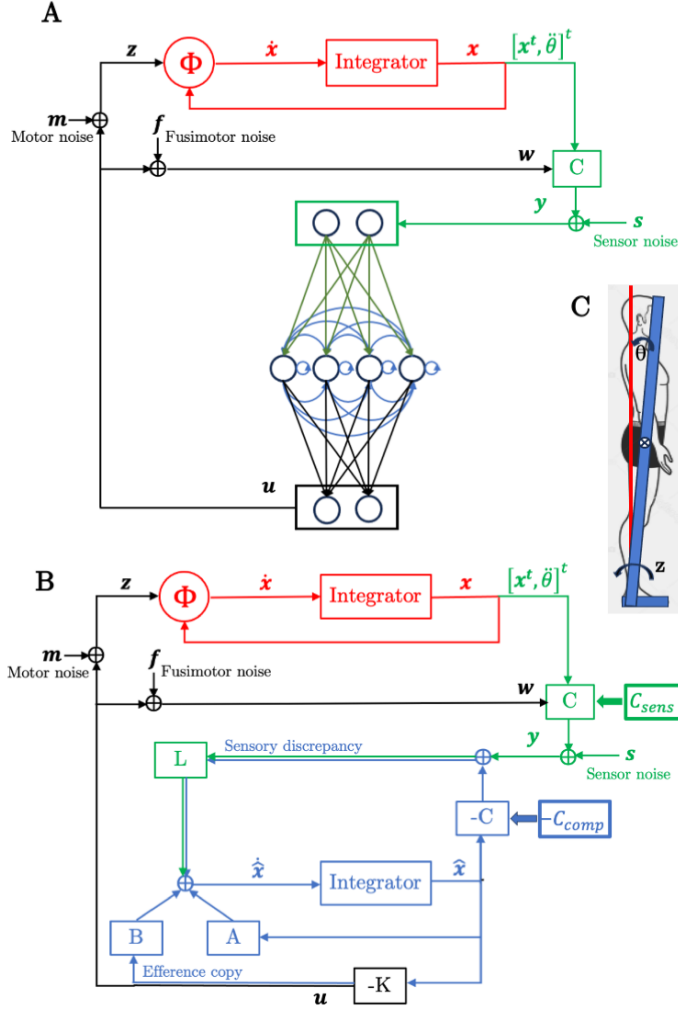


Fig. 1: Closed-loop feedback control model for standing balance. (A)

Block diagram of the closed-loop feedback control model, with a mechanical (in red), a sensory (in green), a computational (multiple colors; see below), and a motor output system (in black). The computational system is a neural network with an input layer with input y , an intermediate layer with recurrent connections, and an output layer with output u . (B) The computational system is based on a linear internal model (approximation) $\dot{x} = Ax + Bz$ of the nonlinear mechanical system $\dot{x} = \Phi(x, z)$ and a sensory internal model C . This assumption, together with an optimality criterion for the control performance (see Eq. 1), defines the weights of the neural network. The matrices L and $-K$ are, respectively, the Kalman and the LQR gain (see text). (C) A standing body with a superimposed compound inverted pendulum rotating about

the ankle, used to model standing balance control. The pendulum's angular position relative to gravity is denoted by θ and the torque at the ankle joint by z .

The sensory system (in green) linearly maps the vectors $[\mathbf{x}^t, \ddot{\theta}]^t$ and \mathbf{w} onto sensory variables, adds noise \mathbf{s} and feeds the resulting \mathbf{y} into the computational system. With respect to these sensory variables, I deviate from the existing literature on closed-loop feedback control, in which the sensory feedback only pertains to the state variables \mathbf{x} . First, I have added the angular acceleration $\ddot{\theta}$ to the state variables \mathbf{x} because this reflects one of the main claims of this paper. Second, I have added the torque variable \mathbf{w} to capture the direct input of the computational (in blue) into the sensory system (in green). In muscle spindles (the main proprioceptive feedback), this direct input is implemented by spinal gamma and beta motor neurons (fusimotor neurons) and is denoted as fusimotor control [3, 7, 8]. The motor output system (in black) adds noise to the computational system's output \mathbf{u} , separately for each of the two pathways: (1) adding motor noise \mathbf{m} (skeletomotor noise plus external perturbations; see further) produces the noisy torque input \mathbf{z} into the mechanical system, and (2) adding fusimotor noise \mathbf{f} produces the noisy torque input \mathbf{w} into the sensory system.

The sensory, motor, and computational system are models of, respectively, the peripheral, somatic, and central nervous system (PNS, SNS, CNS). In this paper, the main interest is in the sensory and the computational system, and I will address the question whether the computational system can control the mechanical system for a plausible sensory feedback and realistic values of the mechanical system's parameters.

The computational system calculates (1) an optimal internal state estimate $\hat{\mathbf{x}}$ by integrating a linear differential equation that takes the sensory feedback \mathbf{y} as input, and (2) an optimal control action \mathbf{u} by multiplying the state estimate $\hat{\mathbf{x}}$ by the gain $-K$. One can consider the computational system both from a neurobiological and an optimal feedback control (OFC) perspective, and these are depicted in, respectively, Fig. 1A and 1B. From the neurobiological perspective, the computational system is a neural network with an input layer, an intermediate layer with recurrent connections, and an output layer. These recurrent connections agree with the fact that, within the CNS, feedback connections are ubiquitous. As is common in neuroscience, I assume that the CNS learns optimal weights for the neural network's connections [14-16]. Calculating these optimal weights is a computational challenge which nowadays is considered a part of machine learning. Here, I take a different approach: I first establish a correspondence between the neural network and the OFC perspective, and then use standard OFC results to express the optimal weights in closed form.

The OFC perspective is model based: the computational system is based on (1) a linear forward model $\dot{\mathbf{x}} = A\mathbf{x} + B\mathbf{z}$ that approximates the nonlinear mechanical system $\dot{\mathbf{x}} = \Phi(\mathbf{x}, \mathbf{z})$, and (2) a linear sensory model $\mathbf{y} = C\mathbf{x} + \mathbf{s}$ of the input to the computational system. I assume the matrices A , B and C to be given and ask for which values of K and L some optimality criterion is achieved. This criterion is a quantification of the person's objective to stay balanced with as little effort as possible. This quantification (J) is a weighted sum of quadratic forms:

$$J = \lim_{T \rightarrow \infty} \frac{1}{T} \mathcal{E} \left(\int_0^T \{[\mathbf{x}(t) - \mathbf{c}]^t Q [\mathbf{x}(t) - \mathbf{c}] + \mathbf{u}(t)^t R \mathbf{u}(t)\} dt \right) \quad \text{Eq. 1}$$

in which $\mathcal{E}()$ denotes expected value, and Q and R are positive definite weight matrices of the appropriate dimensions. The first term

$([\mathbf{x}(t) - \mathbf{c}]^t Q [\mathbf{x}(t) - \mathbf{c}])$ quantifies the difference between the time-varying state variable $\mathbf{x}(t)$ and its target state $\mathbf{c} = [a^+, \mathbf{0}]^t$ (in which a^+ is a small positive number that reflects people's preference for a leaned forward posture), and the second term $(\mathbf{u}(t)^t R \mathbf{u}(t))$ quantifies the energetic cost.

The minimization of J is a well-known problem that has a solution under the following conditions: (1) the mechanical system is linear and identical to the computational system's forward model (i.e., $\dot{\mathbf{x}} = \Phi(\mathbf{x}, \mathbf{z}) = A\mathbf{x} + B\mathbf{z}$), (2) the sensory system's output matrix C is identical to the corresponding matrix of the computational system's sensory model, and (3) the sensor and the motor noise are Gaussian. Together, these conditions and the solution are known as the linear quadratic gaussian (LQG). Optimal control under the LQG is achieved when $-K$ is the linear quadratic regulator (LQR), which depends on A and B (plus the weights Q and R), and L is the Kalman gain, which depends on A and C (plus two noise covariance matrices, which serve as weights) [1].

Applying the LQG results, one can see that the optimal input weights for the neural network are the Kalman gain L , the optimal output weights are the LQR gain $-K$, and the optimal recurrent weights are $A - BK - LC$. With these results, a digital computer does not have to learn the neural network weights from experience with the mechanical system (i.e., a training set). However, for the CNS, learning from experience is the only plausible way. Because this learning process develops over time, the CNS's current weights can only approximate the optimal weights.

It is important to note that the LQG is for continuous signals only, whereas the signals in the peripheral, central and somatic nervous system are sets of spike signals. However, it is possible to formulate a spiking neural network (SNN) with the same functional properties as a LQG

controller [17]. This functional equivalence can be demonstrated using a SNN [18, 19] that produces the type of spiking activity that is observed in biological neural networks: irregular, sparse, and robust.

Actionable sensory feedback

Consider a linear mechanical system with observable states \mathbf{x} . The optimal control action for such a system is the linear combination $-K\mathbf{x}$ [1]. This shows the importance of sensory feedback about the mechanical system's states \mathbf{x} . Optimal control actions can be computed from the sensory feedback not only when the states are observable, but also when the sensory system's output matrix C is invertible. In this case, the optimal control action can be computed as $-KC^{-1}\mathbf{y}$. Sensory feedback obtained via an invertible output matrix C will be called directly actionable (for short, actionable) because a simple linear mapping is sufficient to compute the optimal control action. For actionable feedback, there is no need to pass it through a recurrently connected intermediate layer such as in Fig. 1A.

Non-actionable sensory feedback can be of different types, such as a simple non-invertible mapping of the mechanical system's state \mathbf{x} , or a mapping of non-state variables such as acceleration $\ddot{\theta}$ and torque \mathbf{w} (see Fig. 1A and 1B). In this paper, I will only focus on the latter type. However, it holds for all types of non-actionable sensory feedback that it must be passed through a recurrently connected intermediate layer if it is to be converted into an optimal control action.

Actionable feedback can also profit from a recurrently connected intermediate layer, but only when motor and/or sensory noise is added to the input and/or output of the mechanical system. If the sensory feedback is noisy, more accurate state estimates are obtained by combining the

noisy sensory feedback with model-based predictions using Bayes' rule [20]. Crucially, this can also be performed by the RNN in Fig. 1A, and the optimal combination of the noisy sensory feedback with the model-based predictions is realized by the Kalman gain L . However, for non-actionable sensory feedback, the RNN does not simply improve the accuracy of the state estimates; without the RNN, there would not be any state estimates.

Muscle spindle proprioceptive feedback

Proprioceptive feedback for balance control

Balance control relies on contributions from the somatosensory (including proprioceptive), visual, vestibular and auditory sensory system [2]. When all sensory systems are functioning properly, they work together to maintain balance [21, 22]. In this paper, I focus on proprioceptive feedback about the state variables position and velocity, and muscle spindles are claimed to be the most important sensory organ for this part of proprioception [3]. I will model balance control using only muscle spindle proprioceptive feedback, and by simulating the model I will thus test the hypothesis that this feedback is sufficient for balance control. This is a plausible hypothesis, at least when the support surface is firm and immobile; on such a surface, humans can maintain standing balance after removing vestibular, touch, and visual feedback [4-6].

Muscle spindle feedback is not actionable

For standing balance control, actionable feedback would imply that the muscle spindles provide direct feedback about angular position and velocity. This is a common assumption in the field of standing balance control [2, 21, 23, 24]. However, there is no neurophysiological evidence for

this assumption, and this has been shown in a series of empirical papers that are covered in two specialized review papers [7, 8].

The response properties of muscle spindles are investigated using direct recordings of their output, afferent spikes in sensory neurons. In anesthetized animals, such recordings are obtained from the dorsal horn of the spinal cord [9], and in awake humans from PNS sensory axons using microneurography [7, 25]. A muscle spindle contains the endings of the sensory neurons, and these terminate at so-called intrafusal fibers, which have a sensory function only; the contractile force is produced by the muscle's extrafusal fibers. The sensory neurons' endings respond to the stretch in the intrafusal fibers and if they lie slack (zero tension), the sensory neuron provides no information about the muscle's extrafusal fibers. Usually, a distinction is made between two types of sensory afferents that terminate at different parts of the intrafusal fibers: type Ia or primary afferents terminate at the central region of the intrafusal fibers, and the type II or secondary afferents terminate adjacent to this central region. The dominant view is that primary afferents are more responsive to the dynamics of the stretch, as is reflected in their high sensitivity to acceleration [7, 26].

When discussing the muscle spindles' response properties, it is important to distinguish between active and passive muscles (i.e., muscles that receive neuronal input and those that do not), and if they are active, whether they are moving or stationary.

Recordings in passive muscles

Recordings of passive muscle spindle output are commonly performed using a ramp-and-hold test in which the muscle is stretched from zero

tension to a new length where it is kept stationary for some time [9, 26, 27]. In the first dynamic part of this test (stretch onset; from zero tension to a new length), the firing rates of primary afferents scale with peak acceleration [9]. Acceleration is positive when the muscle is stretched from zero tension to a new length; when acceleration is negative (the muscle decelerates), the primary afferent firing rate drops to zero [9, 26, 27]. Thus, in passive muscles, the primary afferent firing rates scale with the positive part of acceleration.

During the stationary period of the ramp-and-hold test, both primary and secondary afferents have an increased firing rate [9, 26, 27]. During this stationary period, the tension force that was needed to keep the muscle at a constant length, decreases over time and, crucially, the firing rate scales with this muscle tension [9]. The relevance of this observation follows from the fact that, at least in the passive muscle and above the length at which the intrafusal fiber falls slack, muscle tension is roughly proportional to muscle length and this in turn determines joint angle. This potential angular position encoding agrees with several microneurography studies in awake humans: when the muscles are passive, there is an approximately linear relationship between joint angle and sensory neuron firing rate [26, 28-31].

Recordings in active muscles

I first consider active muscles that are either in isometric contraction or moving very slowly. Microneurography recordings during position maintenance and slow tracking movements showed that there is no relationship between joint angular position and firing rate [32, 33]. In these studies, participants were holding a loaded finger at some joint angle, with load being constant and thus independent of joint angle. Thus, muscle

spindles provide length information when the passive joint is moved by an external force, but this information is lost when the joint's position is controlled by the CNS and load cannot be used to infer position.

I now consider recordings from active muscles at movement speeds in the normal range, obtained during naturalistic tasks (reaching, grasping, lifting, key-pressing) and involving muscle spindles in both finger and wrist extensor muscles [34, 35]. Firing rates in both the primary and secondary muscle spindle afferents signaled the velocity of the finger and wrist kinematics, and the primary afferents also signaled acceleration. Crucially, neither primary nor secondary afferents signaled muscle length or the size of the grasped object [34, 35]. These results are consistent with a computational modeling study that demonstrated that the information content in the velocity signal was an order of magnitude larger than that of the position signal [36]. And they are also consistent with the study on slow tracking movements [33]: both primary and secondary afferents increased their firing rates during muscle lengthening, and there was no relation with joint angular position.

A crucial difference between the active and the passive muscle is that, in the former, the muscle spindle intrafusal fibers are activated by spinal fusimotor neurons as a part of fusimotor control. Without fusimotor control, muscle spindle output would only depend on the length of the extrafusal fibers that determine the joint's position. The simplest form of fusimotor control is alpha-gamma coactivation, which effectively deals with the problem that the stretch-sensitive sensory endings have a limited operating range: when the extrafusal fibers contract, the tension in the intrafusal fibers can become too low (they fall slack) for the sensory endings to fire, regardless of the length/velocity/acceleration of the extrafusal fibers. Fusimotor neurons control the length of the intrafusal

fibers, and thereby the sensitivity/gain of the sensory neurons. In alpha-gamma coactivation, the gamma motor neurons fire in sync with the spinal alpha motor (skeletal) neurons, whose firing makes the extrafusal fibers contract. This coordination keeps the intrafusal fibers at a length that keeps the sensory neurons in their operating range.

More complicated forms of fusimotor control have been described and they all involve CNS-level computations that allow for temporal coordination between fusimotor and skeletal neurons [8, 37, 38]. In this paper, I focus on the role of this temporal coordination in distinguishing between reafferent and exafferent feedback. The better the temporal coordination, the more the sensitivity of the sensory neurons shifts to the non-muscular forces, such as gravity, elasticity (which both depend on angular position) and damping (which depends on angular velocity). If the coordination is perfect, then the net forces acting on the intrafusal fibers do not reflect the extrafusal fiber contractions, and the muscle spindle output thus only reflects non-muscular forces. In other words, the muscle spindle feedback is purely exafferent.

In the next section, I will argue that muscle spindles respond to forces via the force-induced accelerations. I will deal with the fact that a subset of these forces are produced by the muscles' extrafusal fibers and therefore may produce reafferent feedback. I will assume that the fusimotor system compensates for the predicted reafferent accelerations in the intrafusal fibers and thereby realizes purely exafferent accelerations in these fibers. Crucially, these exafferent accelerations depend on position- and velocity-related information via position- and velocity-dependent forces. Starting from a mechanical model for standing balance, I will describe the supporting sensory neurophysiological evidence for this hypothesis and will

show how the computational system can extract position- and velocity-related information from these exafferent accelerations.

A mechanical model for standing balance constrains the relation between intrafusal fiber acceleration and the state variables

A mechanical model specifies acceleration components

I now describe a mechanical model for standing balance (the CIP) that can be used to specify the acceleration component to which the muscle spindles respond. The CIP EoM is the following second-order differential equation:

$$I\ddot{\theta} + c_{damp}\dot{\theta} - \frac{1}{2}mgl \sin(\theta) + k_{stiff} \theta = z \quad , \quad \text{Eq. 2}$$

in which m is the mass of the compound pendulum, l is its length, and g is the gravitational constant. The constant I denotes the rotational inertia $I = \frac{1}{3}ml^2$. The ankle joint has both stiffness and damping, and these are characterized by the coefficients k_{stiff} and c_{damp} . The variable z is the forcing torque applied at the ankle. This forcing torque is produced by the muscles' extrafusal fibers and is the sum of a control signal plus motor noise. A critical aspect of Eq 2 is the relation between k_{stiff} and the critical stiffness $\frac{1}{2}mgl$: if $k_{stiff} < \frac{1}{2}mgl$, the CIP is unstable in the upright position (θ accelerates away from 0), and if $k_{stiff} > \frac{1}{2}mgl$, it is stable. Several studies have demonstrated that the ankle joint stiffness k_{stiff} is less than the critical stiffness $\frac{1}{2}mgl$, and that this is due to the compliance of the Achilles tendon [39-42].

I now rewrite Eq. 2 by (1) bringing the state variables to the right side of the equation, and (2) dividing both sides by the rotational inertia I :

$$\ddot{\theta} = I^{-1} \left[-c_{damp}\dot{\theta} + \frac{1}{2}mgl \sin(\theta) - k_{stiff} \theta + z \right] \quad \text{Eq. 3}$$

All terms in Eq. 3 are acceleration components: the terms containing $\dot{\theta}$, $\sin(\theta)$, θ , and z are the acceleration components that are due to, respectively, damping, gravity, elasticity, and the forcing torque, and $\ddot{\theta}$ is the total acceleration. Eq. 3 imposes a constraint on the relation between the variables θ , $\dot{\theta}$, $\ddot{\theta}$ and z , and the computational system can make use of this constraint to extract information about the state variables $\mathbf{x} = [\theta, \dot{\theta}]^t$ from acceleration feedback.

The differential equation in Eq. 3 pertains to a joint that is controlled by multiple muscles, and these are usually grouped functionally as agonists and antagonists. I define the agonists and antagonists as the muscles that produce positive, respectively, negative torque. For the ankle joint, the agonists are responsible for plantar flexion and the antagonists for dorsiflexion. This implies that the forcing torque z in Eq. 3 is the net torque that results from the combined action of both agonists and antagonists.

One-to-one correspondence between angular and translational accelerations

Eq. 3 can be used to specify the acceleration components that are registered by the spindles in the muscles (both agonists and antagonists) that cross the joint at which the forcing torque z is produced. To start out, note that Eq. 3 involves an angular acceleration $\ddot{\theta}$ whereas the muscle spindles respond to translational accelerations in the agonist and antagonist muscles. However, for a given joint, there is a one-to-one correspondence between the joint's angular acceleration $\ddot{\theta}$ and the translational accelerations in the associated muscle-tendon units. The relevant equations depend on where the tendons are attached to the joint's bones, but there is no need to specify this in more detail.

In the following, I will assume that the translational acceleration in a muscle-tendon unit is dominated by the acceleration in its contractile part, the muscle (i.e., the extrafusal fibers). This implies that the tendon may not be so compliant that the muscle's acceleration is absorbed in the tendon. We know that the Achilles tendon is too compliant to keep the body mass over the body's AoS [39-42], but it may not be so compliant that the muscle's acceleration does not dominate the acceleration of the muscle-tendon unit. Under this assumption, there is a one-to-one correspondence between the joint's angular acceleration and the translational accelerations in the associated extrafusal fibers. In the Discussion, I will discuss the consequences of a muscle-tendon unit with a larger tendon compliance.

For three scenarios, I will now describe how Eq. 3 can be used to specify the acceleration components that are registered by the muscle spindles: (1) a passively accelerating joint, (2) an actively accelerating joint, and (3) an active stationary joint (isometric contraction).

Scenario 1: A passively accelerating joint

Because the muscles are passive in this scenario, there is no fusimotor control. Therefore, the linear accelerations of the extra- and the intrafusal fibers are identical, and the one-to-one correspondence also holds between $\ddot{\theta}$ and the translational acceleration of the intrafusal fibers. Because the intrafusal fiber accelerations determine the spindle firing rates, there also is a one-to-one correspondence between $\ddot{\theta}$ and the spindle firing rates in the muscles that are stretched in this acceleration.

For a 1 degree of freedom joint, the neural signal that reflects the angular acceleration $\ddot{\theta}$ is the difference between the firing rates that originate from two populations of sensory neurons, one providing information about the agonist and the other about the antagonist muscle. The firing rates in these populations reflect the positive acceleration in their corresponding muscle, and their difference thus encodes the angular acceleration $\ddot{\theta}$.

Scenario 2: An actively accelerating joint

For this scenario, I assume perfectly coordinated fusimotor and skeletomotor control. I rewrite Eq. 3 by bringing the forcing torque to the left side:

$$\ddot{\theta} - I^{-1}z = I^{-1} \left[-c_{damp}\dot{\theta} + \frac{1}{2}mgl \sin(\theta) - k_{stiff} \theta \right] \quad \text{Eq. 4}$$

In this scenario, the neural signal that informs the CNS about the CIP state is proportional to $\ddot{\theta} - I^{-1}z$. The term $I^{-1}z$ is the contribution of the forcing torque z to the total joint angular acceleration $\ddot{\theta}$, which is related one-to-one to linear accelerations in the agonist and the antagonist extrafusal fibers. Without fusimotor activity, these accelerations would also be present in the intrafusal fibers and would thus cause reafferent feedback. I now assume that the fusimotor neurons generate an acceleration in the intrafusal fibers that cancels this reafferent feedback. Although this intrafusal fiber acceleration is linear, I will represent it by the angular acceleration $-I^{-1}z$ from which the linear accelerations in the agonist and antagonist muscle spindle can be calculated. By taking the difference $\ddot{\theta} - I^{-1}z$, the reafferent feedback is removed from the total acceleration $\ddot{\theta}$, and this results in pure exafferent feedback. This agrees with the fact that the right side of Eq. 3 expresses the same quantity but now as a function of angular position and velocity, which determine the

non-muscular forces gravity, elasticity, and damping that are responsible for the exafferent feedback.

I now relax the assumption that the fusimotor neurons generate an acceleration $-I^{-1}\mathbf{z}$ in the intrafusal fibers that exactly cancels the reafferent feedback. To allow for the fusimotor and the skeletomotor system to generate a different noise, I assume that the fusimotor neurons generate an intrafusal fiber acceleration $-I^{-1}\mathbf{w} = -I^{-1}(\mathbf{u} + \mathbf{f})$, in which \mathbf{f} is the fusimotor noise (see Fig. 1A and 1B). The quantity $I^{-1}\mathbf{w}$ is the predicted reafferent acceleration. In the presence of fusimotor noise, the intrafusal fiber acceleration is $\ddot{\theta} - I^{-1}\mathbf{w}$. Starting from Eq. 4, after some rewriting, this noisy intrafusal fiber acceleration (IFA) can be written as a function of θ , $\dot{\theta}$, \mathbf{m} , and \mathbf{f} :

$$\begin{aligned} IFA(\theta, \dot{\theta}, \mathbf{m}, \mathbf{f}) &= \ddot{\theta} - I^{-1}\mathbf{w} \\ &= I^{-1} \left[-c_{damp} \dot{\theta} + \frac{1}{2} mgl \sin(\theta) - k_{stiff} \theta + \mathbf{m} - \mathbf{f} \right] \end{aligned}$$

The noise in the IFA is the sum of a term that depends on motor noise ($I^{-1}\mathbf{m}$) and one that depends on fusimotor noise ($-I^{-1}\mathbf{f}$). With identical motor and fusimotor noise (i.e., $\mathbf{f} = \mathbf{m}$), the IFA is noise-free, and this drastically improves the performance of the model in the simulations (results not shown); in this paper, I consider the case $\mathbf{f} \neq \mathbf{m}$. Besides $I^{-1}\mathbf{m}$ and $-I^{-1}\mathbf{f}$, the sensory feedback also contains an additional term (\mathbf{s} in Fig. 1B) that reflects the noise in the transduction of the IFA into neuronal firing rates. With respect to the performance of the model, this transduction noise \mathbf{s} cannot be distinguished from the fusimotor noise term $I^{-1}\mathbf{f}$.

The reasoning in the previous paragraph is fully in line with [8, 37, 38] who argued that muscle spindles can be tuned by the CNS via its innervation of the spinal fusimotor neurons. Importantly, the subtraction

of the predicted reafferent feedback goes beyond simple alpha-gamma coactivation which operates at the level of a single muscle. Instead, it is proposed that the CNS combines the planned muscle activations affecting a given joint (both agonists and antagonists) and cancels the resulting reafferent feedback via fusimotor neurons. Consistent with this scheme, it was shown that spindle firing rate was inversely related to the force produced by a non-spindle-bearing muscle [37]. Note that this finding alone does not yet demonstrate that it is caused by a process at the level of the brain.

The model in Fig. 1 considers only a single agonist-antagonist muscle pair and therefore the fusimotor output to the muscle spindles can be represented by a single torque value w . More complicated joint geometries in mechanical systems with multiple rigid bodies (involving between-joint coupling of forces) will require more sophisticated fusimotor output.

$IFA(\theta, \dot{\theta}, m, f)$ encodes three variables: angular position θ , velocity $\dot{\theta}$, and acceleration (the latter via the noise torques m and f). Angular position θ is encoded via the gravitational and the elastic force $\left[\frac{1}{2}mgl \sin(\theta) - k_{stiff} \theta\right]$, which are proportional to θ , after linearizing $\sin(\theta)$. And angular velocity $\dot{\theta}$ is encoded via the damping/viscous force $-c_{damp} \dot{\theta}$, which is proportional to $\dot{\theta}$. The muscle spindle firing rates are proportional to this IFA, and this resolves the apparent contradiction between (1) the muscle spindle being a stretch receptor, responding to force, and (2) the spindle providing information about position and velocity. The resolution is provided by the fact that muscle spindle responds to forces that are proportional to position and velocity.

Acceleration information pertains to the noise accelerations in the intrafusal fibers, and these are produced by the noise torques m and f . There are two sources of motor noise m : skeletomotor noise and external perturbations. There is empirical evidence that they both affect the organism via the induced accelerations. Beginning with skeletomotor noise, this noise co-determines joint angular acceleration $\ddot{\theta}$ and one therefore expects a correlation between $\ddot{\theta}$ and the muscle spindle afferent firing rates, also in the absence of external perturbations. This correlation has been demonstrated for primary afferents in human microneurography studies during unperturbed task performance [34, 35].

Next, external perturbations can be used to investigate the kinematic signal that drives the corrective response. In fact, external perturbations affect the sensory feedback y , and this in turn affects the state estimates \hat{x} and the control action u (see Fig. 1B). The model predicts that corrective responses to external perturbations are driven by acceleration, and this is exactly what has been found for external perturbations of standing balance [43-45]. Crucially, this acceleration-driven component in the corrective responses depends on proprioceptive feedback, because it is only present in animals with intact proprioceptive afferents [43].

The mere fact that corrective responses to an external perturbation are driven by acceleration does not yet demonstrate that these responses are also successful in restoring balance. Here lies an important contribution of the proposed model: $IFA(\theta, \dot{\theta}, m, f)$ not only depends on the external perturbation via the motor noise m but also via the state variables θ and $\dot{\theta}$: these state variables depend on m (which contains the perturbing torque) because m is input to the mechanical system. Because the mechanical system acts as a low-pass filter, the consequences of the motor noise m on the state variables θ and $\dot{\theta}$ remain present for a longer time

than the motor noise itself. This has the important advantage that the computational system can continue to restore the balance when the cause of the imbalance is no longer present.

Scenario 3: An active stationary joint

In this scenario, the joint is not moving but one muscle is actively contracting against an external load. This scenario is typical for standing balance because people prefer a leaned forward posture. In this position, the calf muscles produce a torque that acts against the gravitational torque that results from this posture. In this scenario, $\ddot{\theta} = 0$ and $\dot{\theta} = 0$, from which follows that

$$\begin{aligned} IFA(\theta, \dot{\theta}, m, f) &= I^{-1}w \\ &= I^{-1} \left[\frac{1}{2} mgl \sin(\theta) - k_{stiff} \theta + m - f \right] . \end{aligned}$$

The term $I^{-1} \left[\frac{1}{2} mgl \sin(\theta) - k_{stiff} \theta \right]$ is the IFA that would be observed if there was no muscular torque acting against the net gravitational torque (gravitational torque corrected for stiffness). In the presence of a counteracting muscular torque (the current scenario), the IFA reflects the tension in the intrafusal fibers.

The model predicts that keeping the joint stationary against an external load produces spindle firing rates that are proportional to this load. This prediction is in exact agreement with human microneurography experiments involving stationary joints acting against an external load [27, 46]. This muscle spindle firing under load is even observed in a slowly contracting muscle [33, 47, 48].

The last two scenario's (an actively accelerating and an active stationary joint) can be summarized as follows: muscle spindle afferent firing rates scale with the acceleration that is produced by the non-muscular forces

(accelerating joint scenario), or that would be produced if there was no muscular force working against an external load (stationary joint scenario). The role of fusimotor control is creating the appropriate tension in the intrafusal fibers such that pure exafferent feedback is generated. This exafferent feedback reflects either actual (accelerating joint) or possible (stationary joint) acceleration, but in both scenarios, it scales with the non-muscular forces.

How does the computational system extract state information from the IFA?

The IFA depends on both joint angular position, velocity, and acceleration. Because these components are not separated within the sensory organ (i.e., there are no separate channels for position, velocity, and acceleration), the resulting feedback (muscle spindle afferent firing rates) is not actionable. I now describe how the computational system can extract state information from this mixture of signals.

I assume that the computational system uses a linear approximation of the nonlinear CIP, and I therefore linearize the right side of Eq. 4 (using $\sin(\theta) \approx \theta$ for $\theta \approx 0$). In the approximation, I also ignore the consequences of noise and therefore, on the left side of Eq. 4, I replace z by w :

$$\ddot{\theta} - I^{-1}w \approx I^{-1} \left[-c_{damp}\dot{\theta} + \left(\frac{1}{2}mgl - k_{stiff} \right) \theta \right]$$

In matrix notation:

$$\begin{bmatrix} 1 & -I^{-1} \end{bmatrix} \begin{bmatrix} \ddot{\theta} \\ w \end{bmatrix} \approx \begin{bmatrix} I^{-1} \left(\frac{1}{2}mgl - k_{stiff} \right) & -I^{-1}c_{damp} \end{bmatrix} \begin{bmatrix} \theta \\ \dot{\theta} \end{bmatrix} \quad \text{Eq. 5}$$

The coefficient matrix on the left side of Eq. 5 is the green matrix C in the sensory system of Fig. 1A and 1B, and the coefficient matrix on the right side is the blue matrix C in Fig. 1B. These two matrices will be denoted by, respectively, C_{sens} and C_{comp} . Thus,

$$C_{sens} \begin{bmatrix} \ddot{\theta} \\ \mathbf{w} \end{bmatrix} \approx C_{comp} \begin{bmatrix} \theta \\ \dot{\theta} \end{bmatrix} = C_{comp} \mathbf{x}$$

This shows that there exists a linear combination of the non-actionable sensory feedback variables $\ddot{\theta}$ and \mathbf{w} that equals a linear combination of the actionable state variables \mathbf{x} . The matrix product $C_{comp}\mathbf{x}$ is a sensory internal model [49].

As specified by Eq. 5, the sensory feedback does not pertain to the state variables \mathbf{x} themselves, but to a linear combination of \mathbf{x} . The crucial question is whether the computational system can estimate every state from a time history of this sensory feedback. In the control theory literature, this property is known as observability, and for a linear system it can be assessed from the row space of the so-called observability matrix [50]. Unfortunately, this matrix condition does not tell us whether the mechanical system of interest (the standing body) can be controlled with realistic state and control variables (body angular position, angular velocity, and ankle torques). In this paper, I will use simulation to evaluate whether sensory feedback governed by the matrix pair $[C_{sens}, C_{comp}]$ is sufficient for standing balance control.

An optimal computational system for a linear approximation of the mechanical system

I now describe how to simulate the model in Fig. 1B, and to use these simulations to test whether sensory feedback governed by the matrix pair $[C_{sens}, C_{comp}]$ is sufficient for standing balance control. The rationale for this test is the following: if an optimal computational system with sensory model $C_{comp}\mathbf{x}$ cannot control the CIP with a realistic body sway and ankle torque, then we can rule out the hypothesis that the matrix pair

$[C_{Sens}, C_{Comp}]$ is sufficient for standing balance control. Note that this rationale does not hold if the computational system were suboptimal.

The starting-point are the nonlinear CIP EoM in state-space form, which follow from Eq. 3:

$$\begin{aligned}\dot{\mathbf{x}} = \begin{bmatrix} \dot{\theta} \\ \ddot{\theta} \end{bmatrix} &= \begin{bmatrix} \dot{\theta} \\ I^{-1} \left(-c_{damp} \dot{\theta} + \frac{1}{2} mgl \sin(\theta) - k_{stiff} \theta + z \right) \end{bmatrix} \\ &= \Omega(\mathbf{x}, z)\end{aligned}$$

A linear approximation of $\Omega(\mathbf{x}, z)$ is obtained by taking the first order Taylor expansion around 0 (for θ , $\dot{\theta}$ and z):

$$\begin{aligned}\dot{\mathbf{x}} &\approx \begin{bmatrix} 0 & 1 \\ I^{-1} \left(\frac{1}{2} mgl - k_{stiff} \right) & -I^{-1} c_{damp} \end{bmatrix} \mathbf{x} + \begin{bmatrix} 0 \\ I^{-1} \end{bmatrix} z \\ &\approx A\mathbf{x} + Bz\end{aligned}\tag{Eq. 6}$$

Note that $Bz = B(u + m) = Bu + Bm$, which implies that the system noise (Bm) is a linear function of the motor noise. This follows from the assumption that the mechanical system is deterministic for a given input z because, in that case, the noise in the system's output only depends on the noise in its input.

I now consider optimal control in the sense of Eq. 1 for the following linear dynamical system:

$$\begin{aligned}\dot{\mathbf{x}} &= A\mathbf{x} + Bu + Bm \\ y &= C_{Comp}\mathbf{x} + I^{-1}m - I^{-1}f + s\end{aligned}$$

with Gaussian motor (m) and sensor (s) noise. This optimal control problem is a LQG and its solution is given by a linear differential equation that governs the state estimates $\hat{\mathbf{x}}$:

$$\dot{\hat{\mathbf{x}}} = (A - BK)\hat{\mathbf{x}} + L(y - C_{Comp}\hat{\mathbf{x}})\tag{Eq. 7}$$

in which $-K$ is the LQR gain and L is the Kalman gain, and the control signal u equals $-K\hat{\mathbf{x}}$ [1]. This is the standard solution of the LQG with a few minor adaptations to the usual way of calculating the Kalman gain:

(1) the system noise covariance scaling matrix equals $B\text{var}(m)B^t$ and thus depends on B , (2) the sensor noise covariance scaling matrix contains a term that depends on the fusimotor noise (i.e., $I^{-1}\text{var}(f)I^{-1^t}$), and (3) because the motor (m) and the fusimotor (f) noise can be correlated, this also holds for the system and the sensor noise.

The differential equation in Eq. 7 describes the dynamics of the recurrently connected intermediate layer in Fig. 1A. The weights of the recurrent connections depend on two sets of parameters: (1) A , B and C_{comp} , which characterize the computational system's forward and sensory model, and (2) $-K$ and L , which fulfill the optimality criterion for given A , B and C_{comp} .

Standing balance can be controlled using non-actionable sensory feedback

I now report on a simulation study that evaluates whether OFC with exafferent acceleration feedback can control standing balance with realistic model parameters and realistic kinematic simulation output. In this section, I give a general description of the simulation study; details are given in the Methods. First, the mechanical system (the CIP) is specified by realistic and/or empirical values for its parameters (body length and mass, stiffness, damping). Second, the simulations require noise input and I set the amplitudes of the motor and the fusimotor noise such that their combined effect on the sensory feedback roughly matches the effect of the pure sensory noise: I set the motor noise amplitude such that its contribution to the noise in the sensory feedback equals half the contribution of the pure sensory noise, and I then set fusimotor noise amplitude equal to the motor noise amplitude. The shared variance of the motor and the fusimotor noise is 50%. Third, the LQR gain depends on

the weights of the optimality criterium in Eq. 1 (the 2-by-2 matrix Q and the scalar R) and these are set such that the precision (Q -dependent) and the energetic cost (R -dependent) component have an equal contribution to the optimality criterium.

From a pure computational perspective, there is no limit on the range of torque values that can be used for balance control. However, in the human neuromuscular system, every joint has a torque limit, and I therefore ran simulations in which the output of the computational system was truncated at an empirically determined maximum torque. The maximum ankle torque was set at 195 Nm, a value that was obtained by [51]; if the computational system requested a higher torque value u , it was replaced by this maximum.

There are two requirements for a plausible balance control model: (1) the angular position root-mean-square deviation (RMSD) must converge to zero with decreasing noise amplitude, and (2) the whole RMSD range that is observed empirically must also be produced by the model. There are two empirically determined RMSD maxima (each one corresponding to a noise level): (1) the maximum noise/RMSD for which the computational system can keep the mechanical system's CoG within its AoS (as determined by foot length; see Methods), and (2) the maximum noise/RMSD that humans will tolerate. This second maximum was obtained from a study in which participants had to rely on proprioceptive feedback only (vestibular loss patients with their eyes closed); these participants did not tolerate an angular position RMSD above 1.5 degrees [23, Fig. 4]. Of course, for the model to be plausible, the first maximum RMSD (the RMSD for which the computational system can keep the mechanical system's CoG within its AoS) must be less than this second maximum (1.5 degrees).

Sample results of the simulations are shown in Fig. 2. Panel A shows that (1) the angular position RMSD converges to zero with decreasing noise amplitude, and (2) the CoG moves outside the AoS for a noise level with an angular position RMSD that exceeds the one that can still be tolerated. This result depends on settings (the relative noise amplitudes, the weights of the LQR optimality criterium) that are not fully motivated by empirical results, but it is robust to variations within an order of magnitude, especially for the LQR optimality criterium (results not shown).

Panel B shows the angular position power spectral density (psd) for the noise scale that is marked by a “V” in Panel A. Its shape is remarkably similar to the average psd obtained in a large group of healthy participants [see Fig. 1 in 52]. Panel C shows an example angular position time series for the same noise scale as Panel A. Note the asymmetry around the target angular position, which is a consequence of the gravitational torque pulling the body forward when it is at its target angular position.

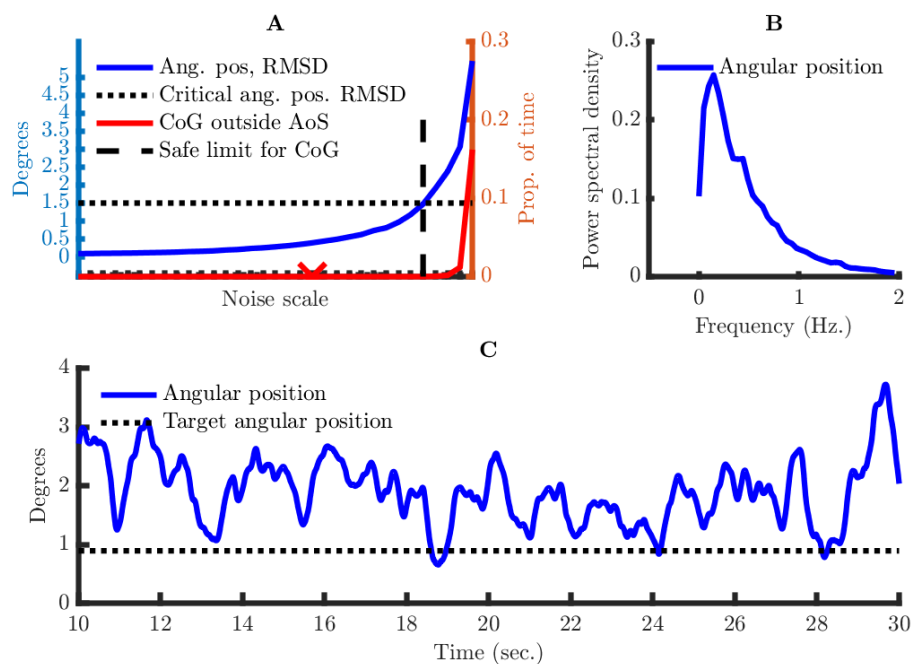


Fig. 2: Simulation results for standing balance control using non-actionable sensory feedback. (A) Two indices of lack of control as a

function of noise: angular position RMSD and the proportion of the time that the angular position exceeds its critical values. The horizontal dotted line indicates the maximum RMSD based on [23], and the vertical dashed line indicates the first noise amplitude for which the computational system cannot keep the mechanical system's CoG within its AoS. (B) Power spectral density of the angular position for the noise scale that is indicated by a red V in panel A. (C) Example angular position time series for the same noise scale as in B.

This simulation study shows that the non-actionable exafferent acceleration feedback is sufficient for controlling standing balance in a realistic way: using realistic parameters for the mechanical system, the computational system keeps the CoG angular position in a realistic regime with respect to angular position RMSD and spectral content.

A general mechanical model constrains the relation between acceleration, force input, and state variables

The simulation study on standing balance control has demonstrated the usefulness of the sensory model $C_{Comp}\mathbf{x}$ to update actionable state estimates using non-actionable proprioceptive feedback. I now discuss the generality of this result, and do this in two steps: (1) I demonstrate the relation between C_{Sens} and C_{Comp} for a general multibody mechanical system (i.e., extending Eq. 5 to a multibody system), and (2) use this relation to demonstrate that a bicycle can be balanced using non-actionable proprioceptive feedback from the rider's upper body.

I start from the following differential equation for a multibody mechanical system:

$$M(\boldsymbol{\theta})\ddot{\boldsymbol{\theta}} + D(\boldsymbol{\theta}, \dot{\boldsymbol{\theta}}) = H\mathbf{z} \quad \text{Eq. 8}$$

The vectors $\boldsymbol{\theta}$, $\dot{\boldsymbol{\theta}}$, $\ddot{\boldsymbol{\theta}}$ and \mathbf{z} are, respectively, the positions, velocities, accelerations and forcing torques of a multibody mechanical system. Because not all joints have to be actuated (see the bicycle model for an example), I use the binary matrix H to distribute the forcing torques over the joints; rows of H that correspond to non-actuated joints are zero. The matrix $M(\boldsymbol{\theta})$ is the mass moment of inertia and the vector $D(\boldsymbol{\theta}, \dot{\boldsymbol{\theta}})$ captures all forces of the non-actuated system (gravity, centrifugal, damping, stiffness). In the CIP, the mass moment of inertia $M(\boldsymbol{\theta})$ is independent of $\boldsymbol{\theta}$ and was denoted by I . Note that Eq. 8 is more general than the familiar manipulator equation form [13], which splits $D(\boldsymbol{\theta}, \dot{\boldsymbol{\theta}})$ into two terms of which one depends on gravity only.

Eq. 8 can be rewritten as follows:

$$\ddot{\boldsymbol{\theta}} - M(\boldsymbol{\theta})^{-1}H\mathbf{z} = -M(\boldsymbol{\theta})^{-1}D(\boldsymbol{\theta}, \dot{\boldsymbol{\theta}}) \quad \text{Eq. 9}$$

I now linearize the left side of Eq. 9 with respect to $\ddot{\boldsymbol{\theta}}$ and $\boldsymbol{\tau}$, and the right side with respect to $\boldsymbol{\theta}$ and $\dot{\boldsymbol{\theta}}$. Next, I evaluate the Jacobian of this linearization at the unstable fixed point $[\boldsymbol{\theta}; \dot{\boldsymbol{\theta}}] = [\mathbf{0}; \mathbf{0}]$. The Jacobian of the left side is $[I, -M(\mathbf{0})^{-1}H]$, in which I is the identity matrix. The Jacobian of the right side requires symbolic differentiation, and the outcome of this operation is denoted by $J_{[\boldsymbol{\theta}; \dot{\boldsymbol{\theta}}]}(\mathbf{0}; \mathbf{0})$. Inserting the linear approximations in the left- and the right side of Eq. 9, one obtains

$$[I, -M(\mathbf{0})^{-1}H] \begin{bmatrix} \ddot{\boldsymbol{\theta}} \\ \mathbf{z} \end{bmatrix} \approx J_{[\boldsymbol{\theta}; \dot{\boldsymbol{\theta}}]}(\mathbf{0}; \mathbf{0}) \begin{bmatrix} \boldsymbol{\theta} \\ \dot{\boldsymbol{\theta}} \end{bmatrix} \quad \text{Eq. 10}$$

The sensory feedback mapping matrices C_{Sens} and C_{Comp} are equal to the Jacobians in, respectively, the left- and the right side of Eq. 10. We thus obtain

$$C_{Sens} \begin{bmatrix} \ddot{\boldsymbol{\theta}} \\ \mathbf{z} \end{bmatrix} \approx C_{Comp} \begin{bmatrix} \boldsymbol{\theta} \\ \dot{\boldsymbol{\theta}} \end{bmatrix}$$

Every row in C_{Sens} specifies the difference between the acceleration at a single joint and a linear combination of the forcing torques. The

corresponding row in C_{Comp} specifies a linear combination of the state variables.

Note that these Jacobians also appear in the linearization of the EoM:

$$\ddot{\boldsymbol{\theta}} = -M(\boldsymbol{\theta})^{-1}D(\boldsymbol{\theta}, \dot{\boldsymbol{\theta}}) + M(\boldsymbol{\theta})^{-1}H\boldsymbol{\tau}$$

$$\ddot{\boldsymbol{\theta}} \approx J_{[\boldsymbol{\theta}; \dot{\boldsymbol{\theta}}]}(\mathbf{0}; \mathbf{0}) \begin{bmatrix} \boldsymbol{\theta} \\ \dot{\boldsymbol{\theta}} \end{bmatrix} + M(\mathbf{0})^{-1}H\boldsymbol{\tau}$$

Thus, the EoM in state-space form, $\begin{bmatrix} \dot{\boldsymbol{\theta}} \\ \ddot{\boldsymbol{\theta}} \end{bmatrix} = \dot{\boldsymbol{x}} = A\boldsymbol{x} + B\boldsymbol{\tau}$, have coefficient matrices A and B , of which the lower halves are equal to, respectively, $J_{[\boldsymbol{\theta}; \dot{\boldsymbol{\theta}}]}(\mathbf{0}; \mathbf{0})$ and $M(\mathbf{0})^{-1}H$. In the Methods section, these lower halves are denoted by A^{lo} and B^{lo} .

Bicycle balance control

I now make use of Eq. 10 to demonstrate that a bicycle can be balanced using non-actionable proprioceptive feedback from the rider's upper body.

Problem definition and bicycle mechanics

There are two important differences between standing and bicycle balance control: (1) a bicycle's AoS is a line instead of a surface, and (2) balance control of a moving bicycle involves not only the gravitational but also the centrifugal force. A stationary bicycle is balanced when the combined CoG of rider and bicycle is above the line that connects the contact points of the two wheels with the road surface, the so-called line of support (LoS). Because of disturbances, this CoG cannot be exactly above this one-dimensional LoS for some time. Therefore, a bicycle is considered balanced if the CoG fluctuates around the LoS within a limited range, small enough to prevent the bicycle from touching the road surface.

On a moving bicycle, not only gravity, but also the centrifugal force acts on the CoG. Crucially, the centrifugal force is under the rider's control via the turn radius [53]. The balance of a moving bicycle depends on the resultant of all forces that act on the CoG: a bicycle is balanced if the direction of this resultant force fluctuates around the LoS within a fixed range. Besides the forces that act on the CoG, there are also forces that are responsible for the turning of the bicycle's front frame, and some of these are independent of the rider's actions [54]. These rider-independent forces are responsible for the bicycle's self-stability and will not be described in detail.

For investigating bicycle balance control, I use the bicycle model in Fig. 3. This model consists of three rigid bodies: front frame, rear frame (which includes the rider's lower body and will also be denoted as such), and the rider's upper body. The positions of these three bodies are specified by three angular variables: steering (δ), lower body (θ_1), and upper body (θ_2) angular position. The lower and upper body angular positions are relative to gravity.

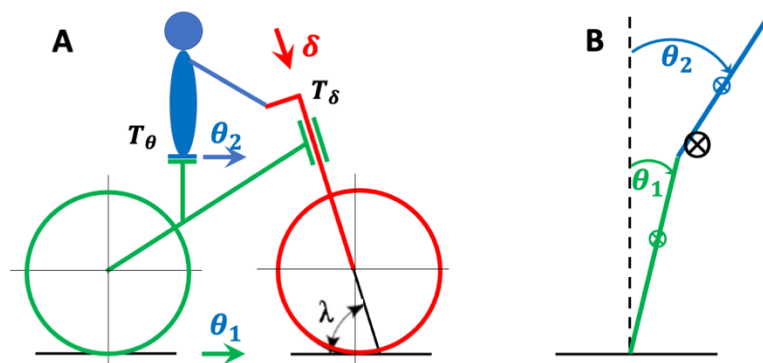


Fig 3: Kinematic variables of the bicycle model plus the rider-controlled forcing torques. (A) Side view. In green, the bicycle rear frame, characterized by its angular position θ_1 over the roll axis (green arrow). In red, the bicycle front frame, characterized by its angular position δ over the steering axis (red arrow). In blue, the rider's upper body, characterized

by its angular position θ_2 over the roll axis (blue arrow). In black, (1) the steering torque T_δ and the pelvic torque T_θ , which are both applied by the rider, and (2) the steering axis angle λ (see text). (B) Rear view. In green, the bicycle rear frame (including the lower body) angular position θ_1 . In blue, the rider's upper body angular position θ_2 . The symbol \otimes denotes the CoG of the upper body (in blue), the lower body (in green), and the combined CoG (in black).

Cycling involves a double balance problem, of which I have only described the first part, which is keeping the combined CoG of rider and bicycle above the LoS. The second balance problem pertains to the rider's upper body only, and it involves keeping the upper body CoG above its AoS, the saddle. I will only consider the balance over the roll axis (parallel to the LoS), which corresponds to upper body movements to the left and the right. I thus ignore the balance over the pitch axis (perpendicular to the LoS and gravity), which corresponds to upper body movements to the front and the back, typically caused by accelerations and braking.

For both balance problems (with respect to the combined and the upper body CoG), the relevant control actions must result in a torque over the roll axis. Within the constraints of our kinematic model, there are two possible control actions: (1) turning the handlebars (using steering torque T_δ), and (2) leaning the upper body (using pelvic torque T_θ). At this point, it is convenient to make use of Fig. 3B, which is a schematic of a double compound pendulum (DCP). By turning the handlebars, the contact point of the front tire (represented by the green rod) with the road surface moves to the left or the right, and this changes the position of the combined CoG relative to the LoS. In the bicycle reference frame (in which the LoS is one of the axes) this corresponds to a centrifugal torque in the direction opposite to the turn (a tipping out torque). Steering in the

direction of the lean produces a tipping out torque that brings the combined CoG over the LoS. This is called steering to the lean/fall.

The second control action is leaning the upper body, which can bring the upper body CoG above the saddle in a direct way. This deals with the second balance problem. However, there is consensus that leaning the upper body cannot deal with the first balance problem (bringing the combined CoG above the LoS), at least not in a direct way. An important argument in favor of this view is that a bicycle with a locked steer cannot be balanced; not a single case has been reported. However, leaning the upper body can deal with the first balance problem in an indirect way: leaning the upper body to one side will make the front and the rear frame lean to the other side (by conservation of angular momentum). Depending on geometrical properties of the bicycle, this rear frame lean may turn the front frame to the same side [54, 55].

What sensory information informs the CNS about the combined CoG angular position?

One of the most challenging aspects of bicycle balance control pertains to the sensory feedback that informs the CNS about the combined CoG angular position. To describe this, it is convenient to repeat Eq. 10:

$$\begin{aligned} [I, -M(\mathbf{0})^{-1}H] \begin{bmatrix} \ddot{\boldsymbol{\theta}} \\ \mathbf{z} \end{bmatrix} &\approx J_{[\boldsymbol{\theta}, \dot{\boldsymbol{\theta}}]}(\mathbf{0}; \mathbf{0}) \begin{bmatrix} \boldsymbol{\theta} \\ \dot{\boldsymbol{\theta}} \end{bmatrix} \\ C_{sens} \begin{bmatrix} \ddot{\boldsymbol{\theta}} \\ \mathbf{z} \end{bmatrix} &\approx C_{comp} \begin{bmatrix} \boldsymbol{\theta} \\ \dot{\boldsymbol{\theta}} \end{bmatrix} \end{aligned}$$

The symbols in this equation map onto the ones in Fig. 3 as follows: $\boldsymbol{\theta} = [\delta, \theta_1, \theta_2]^t$ and $\mathbf{z} = [T_\delta, T_\theta]^t$. Note that the joint between the lower body (rear frame) and the road surface is not actuated, and thus there is no torque that corresponds to θ_1 . Because our bicycle model has less actuators than degrees of freedom, it belongs to the category of underactuated

systems [13]. To control a non-actuated joint, an underactuated system must rely on the actuated joints, and this may be a challenging task for the controller.

The matrices C_{Sens} and C_{Comp} have order 3×5 and 3×6 , respectively. Via the term $I\ddot{\theta}$, every row in C_{Sens} and C_{Comp} corresponds to one of the three joints of the bicycle model: the steering joint (δ), the joint between the road and the lower body (θ_1), and the pelvic joint (θ_2). With respect to proprioceptive feedback at the pelvic joint, only the difference acceleration $\ddot{\theta}_2 - \ddot{\theta}_1$ can be registered (see Fig. 3B). This fact requires matrices C_{Sens} and C_{Comp} with two rows, of which one corresponds to δ and the other to the difference acceleration $\ddot{\theta}_2 - \ddot{\theta}_1$. This is obtained by pre-multiplying the original C_{Sens} and C_{Comp} by the following matrix:

$$\begin{bmatrix} 1 & 0 & 0 \\ 0 & -1 & 1 \end{bmatrix}$$

Thus, no unique information about the lower body (i.e., θ_1) enters the computational system; the corresponding joint is not only non-actuated, but it also sends no unique information about its state to the computational system.

During normal cycling, the lower body is used for propulsion, but it cannot be ruled out that resting on the pedals allows to register balance-relevant sensory information. Therefore, for the purpose of this paper, I consider a restricted form of cycling in which the rider keeps his legs still, does not use them to carry weight, and relies on a motor for propulsion. This is like balance control on a scooter.

I will test the hypothesis that a bicycle can be balanced using the same type of proprioceptive feedback as for standing balance control. The latter involves ankle joint exafferent angular accelerations over the same axis as

the angular position that the person wants to control. In bicycle balance control, there are two controllable joints, the steering axis and the pelvis, but only the latter is over the same axis as the CoG angular position that the rider wants to control. Thus, to test the hypothesis that a bicycle and a standing body can be balanced using the same type of proprioceptive feedback, I ignore the exafferent acceleration feedback from the steering axis. In the simulations on which I will report, this was implemented by pre-multiplying the original C_{sens} and C_{comp} by the vector $[0 \ -1 \ 1]$, which also turns them into vectors. As expected, including the steering axis feedback in the simulations (i.e., not performing the pre-multiplication with $[0 \ -1 \ 1]$) improved the performance of the controller (results not shown). The reported simulation results are thus for a suboptimal scenario, but with the same type of proprioceptive feedback as for standing balance control.

To the best of my knowledge, there is no empirical evidence for the hypothesis that pelvic joint proprioceptive feedback is sufficient for bicycle balance control. However, there are observations that suggest that a bicycle cannot be balanced if the pelvic joint proprioceptive feedback cannot be processed correctly by the rider's internal models. These observations come from a study in which riders were instructed to take turns with a special bicycle (a bricycle) that, on initiation of a turn, tips the rear frame to the outside of the turn, resulting in a lean-induced tipping-out gravitational torque on top of the turn-induced tipping-out centrifugal torque [53, 56]. On a regular bicycle, these two torques act in opposite directions: the turn-induced tipping-out centrifugal torque is cancelled by a lean-induced tipping-in gravitational pelvic torque. Crucially, none of the participants was able to complete a simple obstacle course on the bricycle [53, 56]. This suggests that the non-negotiable tipping-out torque elicits proprioceptive feedback that makes the CNS

think the rider is falling to the opposite side of the initiated turn. Because the CNS has learned to steer to the fall, completing the turn is not possible on the bricycle.

Two bicycle models

Starting from the kinematic bicycle model in Fig. 3, I formulated two sets of EoM for the mechanical system, one nonlinear and one linear. The EoM for both bicycle models are derived in the Methods. The nonlinear EoM are obtained by combining the dynamics of the Acrobot and the double pendulum on a cart under bicycle-specific kinematic constraints [57]. This model is called the Steered Double Pendulum (SDP). The linear EoM are obtained from a linear 2-DoF benchmark model [54] by replacing the rear frame by a linearized double pendulum [57]. This linear model is called the Benchmark Double Pendulum (BDP).

Simulations using the nonlinear EoM of the SDP have the advantage that they mimic the fact that an internal model (linear in our simulations) typically is only an approximation of a nonlinear mechanical system. Simulations using linear EoM will not capture the inevitable differences in the dynamics of the internal and the mechanical model, and a good control performance may thus give an overly optimistic picture.

Simulations using the linear BDP have the advantage that this model captures steering torques that result from the passive (rider-independent) dynamics. Specifically, the model's passive dynamics involves steering torques that depend on the angular position θ_1 (sign and amplitude). These passive steering torques are necessary for the self-stability of the bicycle [54] and they also result in a much more relaxed steering behavior. The SDP does not have these passive steering torques and therefore has a

much twitchier steering behavior, not representative of commercial bicycles. In the BDP but not in the SDP, the rider can in principle feel the angular position through the steering torque, but this potential feedback has been removed from C_{sens} and C_{comp} by pre-multiplying these matrices with $\begin{bmatrix} 0 & -1 & 1 \end{bmatrix}$; the 0 in the first position corresponds to the steering axis.

To be realistic, both the nonlinear and the linear mechanical model must have joints with realistic stiffness and damping. Compared to the ankle joint, much less is known about the stiffness and damping of the steering and pelvic joint. These are not joints in the strict biomechanical sense because they involve more than the interface between two bones; the steering joint involves both the arms and part of the upper body, and the pelvic joint involves both the hip joint (head of femur and acetabulum) and the lumbosacral joint (lumbar spine and sacrum). For the steering joint, I calculated the stiffness from an empirically determined time constant, as described in [57]. And for the pelvic joint, I chose a stiffness coefficient such that the elastic force was 10 percent of the average (over upper and lower body) gravitational force; this allowed the upper and the lower body to fall with different accelerations. The damping ratio for both joints was set at 20, which is a strongly overdamped system. Strong damping was necessary for simulating the SDP; a critical damping ratio of 1 (the minimum damping that is required to suppress the spring-induced oscillations) resulted in numerical inaccuracies in the ODE solver (Matlab's ode45) even at very low noise levels. The BDP could be simulated for a wide range of damping ratio's, including critical damping.

A bicycle can be balanced using non-actionable sensory feedback from the pelvic joint

I followed the same approach as in the simulations of standing balance control, but now the challenge is much more difficult: I try to control a 3-DoF underactuated (instead of a 1-DoF fully actuated) mechanical model using non-actionable feedback from a single joint. As for standing balance control, I assume that the combined effects of motor and fusimotor noise on the sensory feedback roughly matches the effect pure sensor noisy, and to implement this I use as a common scale the noise variance of the sensory feedback. The only difference is that the motor noise is two-dimensional, with a steering and a pelvic component. I assume that the two noise components are independent and have equal variance.

The evaluation of the simulation results is based on the same two requirements as for standing balance control: (1) the combined CoG lean angle RMSD must converge to zero with decreasing noise amplitude, and (2) the whole RMSD range that can be observed must also be produced by the model. There are physical constraints that determine the maximum RMSD: on a bicycle, a combined CoG at some position relative to the LoS can in principle be brought above this LoS by steering, but the maximum combined CoG lean angle for which this is possible depends on speed, turn radius, and the friction between tires and road surface. In [57], it is described (1) how this maximum turn radius can be calculated from speed and the coefficient of friction, and (2) how, for a given bicycle geometry, the corresponding critical steering angle can be calculated. For the speed and the bicycle geometry used in the simulations, this critical steering angle is 18.91 degrees.

The weights of the optimality criterium in Eq. 1 are calculated in the same way as for standing balance control but now using maxima for the lean

and the steering angle, the pelvic and the steering torque. Compared to standing balance control, torque limits are much less important in bicycle balance control. This is because (1) turning the handlebars requires very little torque, and (2) for rotating the upper body there are strong axial muscles, producing a large pelvic torque. As a maximum, I took the torque that is required to keep the upper body in a horizontal position on a Roman chair (a bed with an unsuspended upper body), but this maximum was never reached in the simulations.

The simulations demonstrated that, both for the linear BDP and the nonlinear SDP, the combined CoG lean angle RMSD converged to zero with decreasing noise amplitude. However, compared to the SDP, the BDP could produce much larger RMSD values without becoming uncontrollable and diverging away from the upright position. This is consistent with the much twitchier steering behavior of the SDP, making it harder to control.

Sample results for the BDP are shown in Fig. 4. Panel A shows that the highest value for the combined CoG lean angle RMSD is 2.77 from where it converges to 0 with decreasing noise amplitude. The maximum steering angle observed over the one-minute simulation period increased with noise amplitude, but the critical steering angle of 18.91 degrees was never reached.

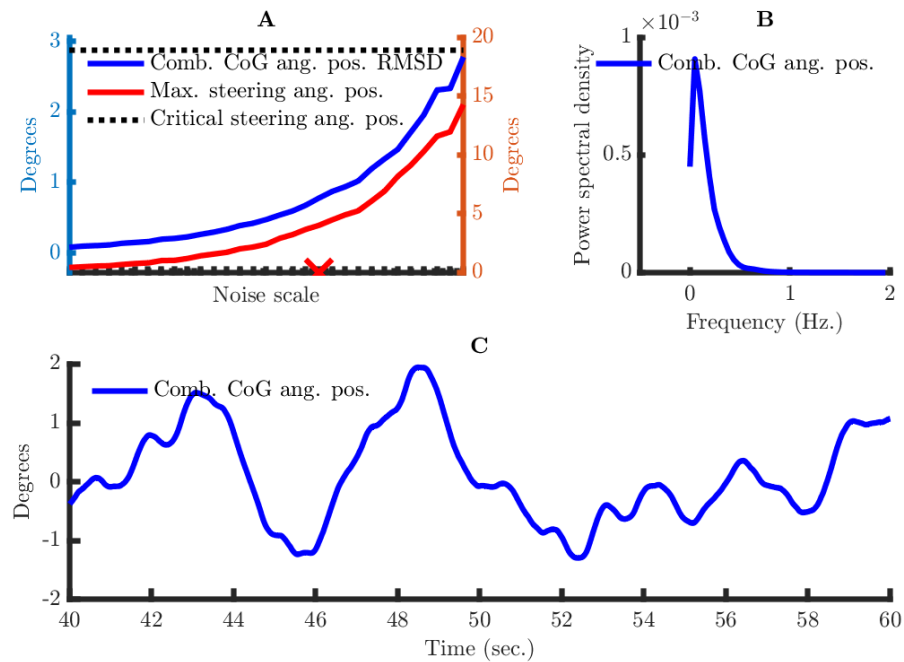


Fig. 4: Simulation results for BDP bicycle balance control using non-actionable sensory feedback. (A) Combined angular position (lean angle) RMSD (in blue), maximum steering angle in a one-minute period (in red), and critical steering angle (in black). (B) Power spectral density of the combined CoG angular position for the noise scale that is indicated by a red V in panel A. (C) Example combined CoG angular position for the same noise scale as in B.

Thus, the non-actionable proprioceptive feedback from the pelvic joint is sufficient to balance a bicycle and, for the BDP, it does so for large part of the range of RMSD values that is theoretically possible. A bicycle can thus be balanced using the same type of proprioceptive feedback as for standing balance control: exafferent angular accelerations over the same axis as the angular position that is to be controlled.

Discussion

Summary of the results

Actionable sensory feedback allows for optimal control actions that are a simple linear combination of this sensory feedback. This holds for all motor tasks with a mechanical system (a human body, a rider-bicycle combination) that is approximately linear in the part of the state space where it stays most of the time, such as in balance control. When the sensory organs only provide non-actionable feedback, these approximately linear mechanical systems allow for an extremely versatile type of control that is based on a CNS-internal dynamical system that estimates the states. This dynamical system can be implemented as a RNN and it uses a sensory model to update the state estimates using non-actionable sensory feedback. The RNN weights are fully specified by a LQG for a given optimality criterion, a forward model of the mechanical system, and a sensory model of the sensory feedback. The relevance of this formalism for motor control crucially depends on the nature of the sensory feedback. I claim that fusimotor control creates the appropriate tension in the intrafusal fibers such that pure exafferent feedback is achieved. This is fully in line with the well-documented properties of muscle spindle afferent firing rates. Specifically, in an accelerating joint, these firing rates scale with the exafferent acceleration that is produced by the non-muscular forces gravity, elasticity, and damping. Alternatively, in a stationary joint, these firing rates scale with the exafferent acceleration that would be produced if there was no muscular force working against an external load. Crucially, although this exafferent acceleration feedback is not actionable, there exists a sensory model that expresses this feedback as a linear function of the state variables. The resulting control mechanism simulates standing and bicycle balance control using realistic parameter values and with forcing torques that are feasible for humans.

Contribution to the modelling of balance control

Several papers in the balance control literature have used an internal dynamical system to model the CNS within the framework of OFC [58-63]. It has been used for testing hypotheses about (1) the information in the sensory feedback (position, velocity, and/or acceleration) that is used for updating the state estimate [58, 59], (2) a mechanism that compensates for the sensorimotor delay [61], (3) intermittent versus continuous standing balance control [60], (4) non-linear components in the corrective responses to balance-perturbing stimuli [62], and (5) the control objective of the CNS (stabilization versus sway minimization) [63]. The main difference with this paper is that it uses OFC to test a hypothesis that is derived from sensory neurophysiology: Is spindle-generated exafferent acceleration feedback sufficient for balance control? Whereas the existing papers mainly demonstrate the scope of OFC in explaining different phenomena [58-63], this paper demonstrates that it continues to be successful if the sensory feedback is highly reduced (only muscle spindle feedback) and constrained to the response properties of the relevant sensory organs.

Short-range muscle stiffness and the mechanics of the muscle spindles

The key neurophysiological claim of this paper is that muscle spindle firing rates reflect the exafferent acceleration component. Because mechanical systems are second order (i.e., the highest derivative in the EoM is 2), acceleration has a well-defined relation with the state variables. From this perspective, the firing rates of a mechanoreceptor may very well be proportional to an acceleration component. However, there is no guarantee that the mechanics of the muscle spindles have the same structure as the mechanics of the limb to which the muscle spindles belong. In fact, there is

good evidence for short-range muscle stiffness that potentially complicates the relation between the two mechanical state variables and spindle output [9, 64-66]. To deal with short-range muscle stiffness, [9] proposed that spindle output scales with a linear combination of the tension force and its first time derivative (yank). However, this same study (on passive muscle spindle output) also demonstrated that peak yank and peak acceleration predicted similar amounts of variance in the initial burst amplitudes [9]. Short-range muscle stiffness is thus consistent with spindle output at stretch onset that scales with peak acceleration. This was also demonstrated by a recent combined biomechanical-neurophysiological model of the muscle spindle that models short-range muscle stiffness at the level of cross-bridge kinetics [67]. This model produces spindle output at stretch onset that scales with peak acceleration.

The model by [67] allows for both skeletomotor and fusimotor input from the CNS and can therefore be used to investigate the claim that spindle feedback scales with the exafferent joint acceleration component. An important question for future research is whether a pattern of combined skeletomotor and fusimotor input can be identified under which this model produces pure exafferent acceleration feedback.

Paradoxical muscle shortening

Pure exafferent feedback effectively deals with the potential problems caused by paradoxical muscle shortening [68-70]. Paradoxical muscle shortening is due to compliance of the Achilles tendon, which makes the body unstable, and necessitates muscle activity to maintain balance. Generating sufficient muscular tension results in paradoxical changes in muscle length: when the body rotates forward ($\dot{\theta} > 0$), the calf muscles are actively shortened (producing a negative torque $\tau < 0$) to maintain

balance. As a result of this paradoxical muscle shortening, muscle length is negatively correlated with angular position [71]. If muscle spindle afferent firing rates would be proportional to muscle length, paradoxical muscle shortening would result in firing rate patterns that are opposite to those of a passive joint that is moved by an external torque. It is unclear how the CNS can interpret such a signal, and this was also noted by [71]. However, if the muscle spindle output reflects the exafferent angular acceleration component, the computational system can rely on a well-defined sensory internal model to successfully update the internal state estimate, as was demonstrated in this paper.

At this point, it is important to discuss the sensory consequences of tendon compliance: the larger the compliance, the less the joint angular acceleration will reflect the extrafusal fiber acceleration. This would reduce the information in the muscle spindle output (which depends on the extrafusal fiber acceleration) about the joint's state (which is constrained by joint angular acceleration via Eq. 3). A principled way to deal with this possible problem (inaccurate information about the joint's state) is by means of a dynamical system for the muscle-tendon unit in which the muscle and the tendons have their own dynamics. Dynamical systems have been used before to model the properties of sensory organs [60-62, 72, 73]. Such a dynamical system would become part of an extended mechanical system with additional output variables: lengths, velocities, and accelerations of the individual muscles (extrafusal fibers), both agonists and antagonists, and their corresponding tendons. The extrafusal fiber accelerations then co-determine (together with the fusimotor output to the intrafusal fibers) the muscle spindle firing rates. Note that, if the mechanical system is extended by a component for the muscle-tendon dynamics, also the computational system is extended by an internal model for this component.

Central mechanisms for cancelling re-afferent feedback

Purely exafferent muscle spindle feedback requires perfectly coordinated fusimotor and skeletomotor control. It is difficult to argue that this is always the case, especially because the computational system must learn to compute fusimotor output that cancels possible reafferent feedback. Thus, the feedback may also contain a reafferent part, and this can be made precise from Eq. 2 if the forcing torque is split in a part that is matched by fusimotor control (FMC) and a part that is not: $z = u^{FMC} + u^{nonFMC} + m$. The matched part u^{FMC} corrects the intrafusal fiber acceleration for the component $-I^{-1}u^{FMC}$ that would become reafferent without fusimotor control. The remainder acceleration component $-I^{-1}u^{nonFMC}$ specifies the reafferent part of the sensory feedback and goes to the right of the equation. Central mechanisms exist via which re-afferent feedback can be cancelled [74, 75] and they depend on a corollary discharge, an efference copy with a special role in the processing of sensory feedback. Similar mechanisms might also be used to cancel the reafferent acceleration component $-I^{-1}u^{nonFMC}$.

Non-actionable feedback in the vestibular system

I will investigate whether actionable feedback is also a useful concept in the vestibular system. From the perspective of balance control, vestibular feedback would be actionable if it informs the CNS about the body's tilt (roll and pitch) relative to gravity. The vestibular system literature is very aware of the limits on the information that is encoded in the sensory afferents [76-80]. Although the concept of actionable feedback (its formal definition and motivation from OFC) is absent in the vestibular system literature, much of the thinking is inspired by the fact that the output of

the vestibular sensory organs (otoliths and semicircular canals) is only useful if it allows for balance control.

Otolith afferent fibers are sensitive to head tilt [76-78] via the gravitational force that acts on the endolymph fluid and could thus in principle provide actionable feedback. However, an organ that is sensitive to gravitational force is also sensitive to forces that cause translational acceleration.

Crucially, according to Einstein's equivalence principle, such an organ cannot discriminate between these two types of force [76, 79, 80]. This is denoted as gravito-inertial ambiguity, and it implies that pure otolith feedback cannot be relied upon for balance-restoring control actions.

Recent evidence has shown that a subset of the otolithic afferents (the regular firing afferents) are much more sensitive to sustained tilt than to brief translational accelerations [78], restricting the gravito-inertial ambiguity to very slow accelerations, but not resolving it.

The dominant hypothesis about the resolution of the gravito-inertial ambiguity is that the CNS combines information from the otoliths and the semi-circular canals to separate tilt from translational acceleration [73, 77, 81-87]. That work is closely related to the present paper. The starting point is that the canal feedback is a high pass filtered angular velocity signal, with the filtering being due to the inertia of the endolymph fluid and its friction with the interior of the canals. This feedback is non-actionable but a clever integration produces an outcome that approximately encodes tilt [77]. This clever integration can be considered as an inversion of a sensory model that specifies how canal afferent feedback depends on tilt. As in every noisy integration, drift may occur, and multisensory integration (using visual and/or otolith information) is necessary to correct for it [77].

This inverse sensory model differs from the computational system in Fig. 1B in two ways. First, the computational system uses a sensory forward model (instead of an inverse model) specified by C_{Comp} to compute the sensory consequences of the current state estimates. The role of the inverse sensory model is now for the Kalman gain which maps the sensory feedback onto an update of the current state estimate. Second, the sensory model in this paper is a simple linear mapping of the state variables instead of a dynamical system that describes the intra-sensor (canal) dynamics (i.e., high pass filtering of the velocity signal). However, [73] demonstrated how the computation by the inverse sensory model can be performed by a Kalman filter combined with a forward sensory model that specifies the canal dynamics. In one sense, this is an extension of the model in Fig. 1B because the dynamics-free linear mapping C_{Sens} is replaced by a dynamical system that describes the filter characteristics of the canals. In the same way, it would in principle be possible to specify the dynamics inside the muscle spindles that are responsible for transducing the exafferent acceleration component into action potentials. Such an extended model involves two states, the state of the mechanical and the state of the sensory system. Note that this is the same type of solution as for the problems that may be caused by the different dynamics of the two components of the muscle-tendon unit. In another sense, the model by [73] is a reduced version of the model in Fig. 1B, because it is open loop: the model produces sensory feedback from noisy motor input, but the motor commands do not depend on state estimates. Thus, the model by [73] is unrelated to OFC.

In the previous, I have tacitly assumed that head tilt is identical to body tilt, and this is the case if the body rotates over the ankle axis without a bend in the neck, pelvis, or knees. I now drop this assumption, and this immediately points to an important difference between muscle spindle and

vestibular feedback: the former can be attributed to a specific joint (i.e., the joint that is controlled by the spindle-containing muscles) whereas the latter is ambiguous in that respect. Specifically, a tilt of the canals and the otoliths can be due to a rotation at any of the four joints, neck, pelvis, knees, and/or ankles. In principle, this ambiguity can be resolved by multisensory integration involving proprioceptive feedback from these four joints. This has been demonstrated for the neck joint by [22] using an approach that can in principle be extended to all four joints. The approach of [22] is based on the assumption (subsequently verified) that multisensory integration obeys Bayes' rule. Our model can be extended to multiple sensory feedback channels such as muscle spindles from multiple joints and vestibular feedback, assuming a sensory model is available. The resulting multisensory integration would also obey Bayes' rule in the same sense as the Kalman filter is a special case of recursive Bayesian estimation (with the prior being the posterior of the previous time step).

Head rotations can result from both external and self-generated (muscular) forces, and for the CNS it is essential to distinguish between the corresponding sensory feedback (resp., exafferent and reafferent). Although the vestibular sensory afferents do not distinguish between active and passive movements, many studies have demonstrated that brainstem and cerebellar neurons show a reduced firing rate during active as compared to passive movements [see refs in 73, 88]. An ingenious study by [89] demonstrated that, during active movements, the firing rate did not simply reflect the exafferent component but inhibited the vestibular input if the proprioceptive feedback of the self-motion could be predicted. When active and (unpredictable) passive motion were combined, resulting in activation of the same muscle proprioceptors, then brainstem vestibular neurons encoded the total vestibular input, rather than the exafferent input alone.

This pattern of results is consistent with the role of an internal model of the sensory consequences of active head motion that suppresses reafferent vestibular feedback if the neck proprioceptive feedback matches the prediction of the internal model. A likely candidate for this suppression are cerebellar neurons, which have been shown to encode the prediction error [90]. Note that exafferent muscle spindle feedback also encodes prediction error: via fusimotor neuronal activity the predicted acceleration of the intrafusal fibers is subtracted from the total acceleration. Thus, an alternative route for the suppression of the brainstem vestibular neurons could be muscle spindle feedback, with suppression being triggered by the absence of muscle spindle feedback.

More complex mechanical systems

My model for balance control is general in the sense that it only depends on the mechanical system's EoM and some parameters for which realistic values can be found (see Methods). However, because the mechanical system may be complex, it may be difficult to obtain its EoM. Therefore, in this paper, I considered a restricted form of cycling in which the rider keeps his legs still, does not use them to carry weight, and relies on a motor for propulsion. Under these restrictions, I could derive two sets of EoM for the rider-bicycle combination, the BDP and the SDP. However, most cyclists transfer a large part of their weight to the pedals and the handlebars; downhill mountain bikers (the balance artists in the cycling community) even do this for the full 100 percent. To model bicycle balance control with less constraints on the rider's movements, we need EoM for a more general mechanical system in which (1) the lower body is no longer a part of the rear frame, and (2) the AoS for the combined upper and lower body is formed by saddle, pedals, and handlebars. For the rest of the

model (sensory, computational, and motor output system), no new ingredients are needed.

Conclusion

This paper integrates theoretical views from motor control with experimental results from sensory neurophysiology and applies the resulting model to balance control. The result is a dynamical system that estimates the full state using non-actionable feedback (the exafferent acceleration component) and uses this estimate to successfully control the balance of a standing body and a rider-bicycle combination.

Methods

Matlab toolbox

All simulations were performed using the Matlab Balance Control (BalCon) toolbox that is shared in the supplementary information, together with the scripts that produced the simulation results, including the figures. For every mechanical system, the BalCon toolbox contains one function that computes the EoM and their linearization. Most of the toolbox's functions are generic, in the sense that they can be used for all mechanical systems.

Simulations of standing balance control

The computer simulations are based on difference equations that are discrete time versions of the differential equations that were presented in the Results section. The difference equations for the linear dynamical system under consideration are the following:

$$\begin{aligned}\mathbf{x}_{k+1} &= A_{dt}\mathbf{x}_k + B_{dt}\mathbf{u}_k + B_{dt}\mathbf{m}_k \\ y_k &= C_{Comp}\mathbf{x}_k + B_{dt}^{lo}\mathbf{m}_k - B_{dt}^{lo}\mathbf{f}_k + s_k\end{aligned}$$

In this equation, k indexes discrete time steps that are separated by a time interval dt . The matrices A_{dt} and B_{dt} are obtained from the well-known solution of a linear differential equation: $A_{dt} = e^{A_{cont}dt}$ and $B_{dt} = A_{cont}^{-1}(A_{dt} - I)B_{cont}$ [91]. The lower half of B_{dt} is denoted by B_{dt}^{lo} . The use of B_{dt}^{lo} instead of the inverse mass moment of inertia I^{-1} is explained in *A general mechanical model constrains the relation between acceleration, force input, and state variables*.

Optimal control is provided by the discrete time version of Eq. 7:

$$\hat{\mathbf{x}}_{k+1} = (A_{dt} - B_{dt}K_{dt})\hat{\mathbf{x}}_k + L_{dt}[y_k - C_{Comp}(A_{dt} - B_{dt}\hat{\mathbf{x}}_k)]$$

The mechanical system (the CIP) is specified by realistic and/or empirical values for its parameters: body length $l = 1,85$ m., body mass $m = 85$ kg., gravitational constant $g = 9,8066$, ankle stiffness $k_{stiff} = 493.4706$ Nm/rad. (64% of the critical stiffness), and ankle damping $c_{damp} = 30$ Nm/(rad./s) [42]. These parameter values also specify the linear approximation in Eq. 6. The CIP dynamics are simulated by the Matlab function ode45, which is based on an explicit Runge-Kutta (4,5) formula [92]. As depicted in Fig. 1, the input to the mechanical system is $z_k = u_k + m_k$, with $u_k = -K_{dt}\hat{x}_k$, and the output is $[\mathbf{x}_{k+1}^t, \ddot{\theta}_{k+1}]^t$.

The feedback loop is closed by the sensory system that maps the output of the mechanical system ($\ddot{\theta}_{k+1}$), the output of the fusimotor system (w_{k+1}), and the pure sensory noise (s_{k+1}) to the sensory feedback y_{k+1} :

$$y_{k+1} = C_{Sens} \begin{bmatrix} \ddot{\theta}_{k+1} \\ w_{k+1} \end{bmatrix} + s_{k+1}$$

To simulate CIP dynamics under closed-loop feedback control, one must add noise. I set the noise parameters such that the effects of motor and pure sensor noise on the sensory feedback are equal. As a common scale for the effects of these three noise types, I use the noise variance of the sensory feedback y_k : if the noise source is only sensory, then $var(y_k) = var(s_k)$, and if the noise source is only motor, then

$$var(y_k) = B_{dt}^{lo} var(m_k) B_{dt}^{lo t} + C_{Comp} B_{dt} var(m_k) B_{dt}^t C_{Comp}^t \quad \text{Eq. 11}$$

In the simulations, I start from a noise scaling variable σ and (1) set $var(s_k) = \sigma$, (2) scale $var(m_k)$ such that the expression on the right side of Eq. 11 equals σ , and (3) set $var(f_k) = var(m_k)$. I set the covariance $cov(m_k, f_k)$ such that the shared variance of m_k and f_k is 50%.

The variance of the noise terms $B_{dt}m_k$ (for the state equation, but also fed into the output equation) and $-B_{dt}^{lo}f_k + s_k$ (for the output equation only) and their covariance are used as weights in the calculation of the Kalman gain L_{dt} . This Kalman gain is a part of the computational system, and we thus implicitly assume that the CNS learns the sensor and the motor noise amplitudes (properties of the PNS and SNS) from experience.

To be realistic, the ankle torque in the simulations must be less than the maximum voluntary contraction (MVC) of the ankle muscles. Therefore, the output of the computational system is truncated at an empirically determined MVC. Because humans prefer a leaned forward position, I use plantarflexion MVC. In a study with 20 participants, the mean plantarflexion MVC was estimated to be 195 Nm [51].

In the simulations, I evaluate whether the CoG remains over the AoS, which is a fraction of the sole length. To determine the AoS, I use a body-to-sole-length ratio of 6.6 [93], place the ankle at 25% from the rear end of the sole, and assume that the CoG must remain at 10% from the front and the rear end of the sole. The latter assumption is required because there can be no reaction forces near the edge of the sole. This results in a critical angular position interval $[-0.0758, 0.2293]$ rad. over the ankle joint.

The LQR gain K_{dt} depends on the weights of the optimality criterium in Eq. 1, the 2-by-2 matrix Q and the scalar R . These weights are set such that the precision (Q -dependent) and the energetic cost (R -dependent) component have an equal contribution to the optimality criterium. In this calculation, I set $c = [0.0156 \quad 0]^t$ rad., in agreement with the observation that humans prefer a leaned forward position around 0.0156 rad. [94]. I use the maximum metric to calculate a diagonal matrix Q and a scalar R that produce equal values for $\mathbf{x}_{max}^t Q \mathbf{x}_{max}$ and $u_{max} R u_{max}$. For the calculation

of \mathbf{x}_{max} , I start from the critical angular position interval $[-0.0758, 0.2293]$ rad., and calculate the critical angular velocity from the maximum angle position frequency of 1.875 Hz reported in [52]. This results in $\mathbf{x}_{max} = [0.2137 \quad 0.3655]^t$. I give angular position and angular velocity an equal contribution to the precision component by setting Q_{11} and Q_{22} such that $0.2137^2 Q_{11} = 0.3655^2 Q_{22}$. The critical torque $u_{max} = 195$ is obtained from [51].

The SDP EoM

The SDP EoM can be assembled from three components: (1) the EoM of a double compound pendulum with an actuated base (like the double compound pendulum on a cart, DCPC) and an actuated pelvic joint (like the Acrobot), (2) a planar kinematic bicycle model [95] that produces a formula for the acceleration at this base, and (3) a torsional spring-mass-damper system for the steering angle. Specifically, I model the angular positions θ_1 and θ_2 as the result of a double compound pendulum on a (zero-mass) cart (DCPC) and acceleration equal to $\alpha(\delta)$, the centrifugal acceleration derived under the planar kinematic bicycle model (see further). The EoM for this DCPC can be written as follows:

$$\begin{aligned} & \begin{bmatrix} d_1 \cos(\theta_1) \\ d_2 \cos(\theta_2) \end{bmatrix} \alpha(\delta) + \begin{bmatrix} d_3 & d_4 \cos(\theta_1 - \theta_2) \\ d_4 \cos(\theta_1 - \theta_2) & d_5 \end{bmatrix} \begin{bmatrix} \ddot{\theta}_1 \\ \ddot{\theta}_2 \end{bmatrix} & \text{Eq. 12} \\ & + \begin{bmatrix} 0 & d_4 \sin(\theta_1 - \theta_2) \theta_2 \\ d_4 \sin(\theta_1 - \theta_2) \phi_1 & 0 \end{bmatrix} \begin{bmatrix} \dot{\theta}_1 \\ \dot{\theta}_2 \end{bmatrix} \\ & + \begin{bmatrix} -f_1 \sin(\theta_1) \\ -f_2 \sin(\theta_2) \end{bmatrix} \\ & + \begin{bmatrix} k_{pelvis}(\theta_1 - \theta_2) + c_{pelvis}(\dot{\theta}_1 - \dot{\theta}_2) \\ -k_{pelvis}(\theta_1 - \theta_2) - c_{pelvis}(\dot{\theta}_1 - \dot{\theta}_2) \end{bmatrix} = \begin{bmatrix} 0 \\ T_\theta \end{bmatrix} \end{aligned}$$

These EoM are obtained by first applying the Euler-Lagrange method to the DCPC with a zero-mass cart, and then adding the constraint that the cart is controlled by the steering-induced centrifugal acceleration $\alpha(\delta)$.

The derivation of the DCPC EoM using the Euler-Lagrange method can be found in the literature. Here, I started from Bogdanov (96) and added stiffness (with constant k_{pelvis}), damping (with constant c_{pelvis}) and torque input T_θ at the pelvic joint (between the upper and the lower body), similar to the Acrobot [13]. Next, I added the constraint that the angles θ_1 and θ_2 have no direct effect on the position of the base of the first rod (in the DCPC, the point where the cart is attached). This constraint follows from the fact that the bicycle's wheels are oriented perpendicular to the cart's wheels. Under this constraint, the position of the base of the first rod is fully controlled by the steering-induced centrifugal acceleration $\alpha(\delta)$.

The constants in Eq. 12 are defined as follows:

$$\begin{aligned}
 d_1 &= m_1 l_1 + m_2 L_1 \\
 d_2 &= m_2 l_2 \\
 d_3 &= m_1 l_1^2 + m_2 L_1^2 + I_1 \\
 d_4 &= m_2 L_1 l_2 \\
 d_5 &= m_2 l_2^2 + I_2 \\
 f_1 &= (m_1 l_1 + m_2 L_1)g \\
 f_2 &= m_2 l_2 g
 \end{aligned}
 \tag{Eq. 13}$$

The constants m_1 , L_1 , l_1 and I_1 are, respectively, the mass, the length, the CoG ($L_1/2$) and the mass moment of inertia of the double pendulum's first rod, which represents the bicycle and the rider's lower body. The constants m_2 , L_2 , l_2 and I_2 are defined in the same way, but now for the second rod, which represents the rider's upper body. Finally, g is the gravitational constant.

I now give the formula for the centrifugal acceleration $\alpha(\delta)$ that can be derived from a well-known planar bicycle model from the vehicle dynamics literature [95]:

$$\alpha(\delta) = v^2 \frac{\cos(\beta(\delta))}{W} \tan(\delta)$$

This formula depends on the speed v , the bicycle wheelbase W , and the so-called slip angle $\beta(\delta)$, which is the angle between the velocity vector of the combined CoG and the LoS. This slip angle can be obtained as follows:

$$\beta(\delta) = \tan^{-1} \left(\frac{w_r \tan(\delta)}{W} \right)$$

In this equation, w_r is the position of the combined CoG on the LoS. More precisely, w_r is the distance between the road contact point of the rear wheel and the orthogonal projection of the combined CoG on the LoS. For realistic values ($W = 1.02$, $w_r = 0.3$, $-20^\circ < \delta < 20^\circ$), the slip angle $\beta(\delta)$ is almost a linear function of δ :

$$\beta(\delta) \approx \frac{w_r \delta}{W}$$

For steering angles $-20^\circ < \delta < 20^\circ$, all deviations from linearity are less than 0.36%. In my simulations, I have used this approximation.

Finally, I introduce the model for the steering angle δ . This model assumes that the steering angle is fully controlled by rider-applied forces on the handlebars; I thus ignore all forces that may contribute to a bicycle's self-stability. The steering assembly consists of the front wheel, the fork, the handlebars, and the rider's arms. I model this assembly as a torsional spring-mass-damper system:

$$I_{steer} \ddot{\delta} + c_{steer} \dot{\delta} + k_{steer} \delta = T_\delta \quad \text{Eq. 14}$$

In this equation, I_{steer} is the assembly's rotational inertia, c_{steer} its damping, and k_{steer} its stiffness. The input to the steering assembly is the net torque produced by the rider's arm muscles and denoted by T_δ .

It is possible to derive expressions for the second derivatives $\ddot{\delta}$ and $[\ddot{\theta}_1, \ddot{\theta}_2]^T$ from Eq. 12 and Eq. 14. These expressions are complicated and not insightful. In my simulations, I use these expressions to define the

state-space equations $\dot{\mathbf{x}} = \Omega(\mathbf{x}, \mathbf{u} + \mathbf{m})$ for the state variables $\mathbf{x} = [\delta, \theta_1, \theta_2, \dot{\delta}, \dot{\theta}_1, \dot{\theta}_2]^T$, external torques $\mathbf{u} = [T_\delta, T_\theta]^T$, and motor noise \mathbf{m} .

The BDP EoM

The BDP is based on three ideas. The first idea is to follow the approach of [54] and derive linearized EoM for a bicycle with the rider's lower body rigidly attached to the rear frame and no upper body. These linearized EoM depend on a number of constants, and I chose these constants such that (1) the front frame is as similar as possible to the self-stable benchmark bicycle model described by [54], and (2) the lengths and masses are as similar as possible to the SDP. The second idea is to model the interactions between the upper body and the rear frame (which includes the lower body) by the linearized EoM of the double compound pendulum, similar to [97]. Finally, the third idea is to first derive the BDP EoM without stiffness and damping terms, and to add these terms only in the last step.

The approach of [54] involves a method to calculate the defining matrices of linearized EoM of the following type:

$$\mathbf{M} \begin{bmatrix} \ddot{\delta} \\ \ddot{\theta}_1 \\ \ddot{\theta}_2 \end{bmatrix} + \mathbf{C} \begin{bmatrix} \dot{\delta} \\ \dot{\theta}_1 \\ \dot{\theta}_2 \end{bmatrix} + \mathbf{K} \begin{bmatrix} \delta \\ \theta_1 \\ \theta_2 \end{bmatrix} = \mathbf{0}$$

The matrices \mathbf{M} , \mathbf{C} and \mathbf{K} are functions of several constants (angles, lengths, masses, mass moments of inertia, gravitational acceleration, speed) that characterize the bicycle components and the internal forces that act on them. However, [54] only derived linearized EoM for bicycles with a rider that was rigidly attached to the rear frame. Thus, the upper body angular position θ_2 is absent from their EoM. This missing component can be obtained by linearizing the double pendulum EoM which models the

interactions between θ_1 and θ_2 . Schematically, each of the matrices \mathbf{M} , \mathbf{C} and \mathbf{K} is composed as follows:

$$\begin{bmatrix} \text{MP}(1,1) & \text{MP}(1,2) & 0 \\ \text{MP}(2,1) & \text{MP}(2,2) & 0 \\ 0 & 0 & 0 \end{bmatrix} + \begin{bmatrix} 0 & 0 & 0 \\ 0 & \text{DP}(1,1) & \text{DP}(1,2) \\ 0 & \text{DP}(2,1) & \text{DP}(2,2) \end{bmatrix}$$

in which ‘‘MP’’ denotes ‘‘Meijaard, Papadopoulos et al’’ [54], and ‘‘DP’’ denotes ‘‘Double Pendulum’’. The MP calculations were performed by means of the Matlab toolbox Jbike6 [98], in which I entered the constants for a bicycle with the rider’s lower body rigidly attached to the rear frame and no upper body. This produced the constants $\text{MP}(i, j)$ ($i, j = 1, 2$) for \mathbf{M} , \mathbf{C} and \mathbf{K} .

I now model the interactions between the upper body and the rear frame by the linearized EoM of the double compound pendulum. The nonlinear EoM of the double compound pendulum are obtained from Eq. 12 by removing the terms that correspond to the centrifugal acceleration $\alpha(\delta)$, the stiffness and the damping:

$$\begin{aligned} & \begin{bmatrix} d_3 & d_4 \cos(\theta_1 - \theta_2) \\ d_4 \cos(\theta_1 - \theta_2) & d_5 \end{bmatrix} \begin{bmatrix} \ddot{\theta}_1 \\ \ddot{\theta}_2 \end{bmatrix} \\ & + \begin{bmatrix} 0 & d_4 \sin(\theta_1 - \theta_2) \theta_2 \\ d_4 \sin(\theta_1 - \theta_2) \theta_1 & 0 \end{bmatrix} \begin{bmatrix} \dot{\theta}_1 \\ \dot{\theta}_2 \end{bmatrix} + \begin{bmatrix} -f_1 \sin(\theta_1) \\ -f_2 \sin(\theta_2) \end{bmatrix} \\ & = \begin{bmatrix} 0 \\ T_\theta \end{bmatrix} \end{aligned}$$

I evaluate these EoM at $\theta_1 = \theta_2$ and replace $\sin(x)$ by its linear approximation near 0: $\sin(x) \approx x$. This results in

$$\begin{bmatrix} d_3 & d_4 \\ d_4 & d_5 \end{bmatrix} \begin{bmatrix} \ddot{\theta}_1 \\ \ddot{\theta}_2 \end{bmatrix} + \begin{bmatrix} -f_1 & 0 \\ 0 & -f_2 \end{bmatrix} \begin{bmatrix} \theta_1 \\ \theta_2 \end{bmatrix} = \begin{bmatrix} 0 \\ T_\theta \end{bmatrix}$$

The constants d_3, d_4 and d_5 contain elements that must be added to the matrix \mathbf{M} , and the constants f_1 and f_2 contain elements that must be added to the matrix \mathbf{K} (for the definitions, see Eq. 13). I will use the notation $\text{DP}(i, j)$ ($i, j = 1, 2$) to denote these elements. For \mathbf{M} , the following elements are added:

- $\text{DP}(1,1) = m_2 L_1^2$

- $DP(1,2) = DP(2,1) = d_4 = m_2 L_1 l_2$
- $DP(2,2) = d_5 = m_2 l_2^2 + I_2$

And for \mathbf{K} , the following elements are added:

- $DP(1,1) = m_2 L_1 g$
- $DP(2,2) = -f_2 = -m_2 l_2 g$

Finally, I added stiffness and damping terms that were also added to the SDP. The stiffness and damping terms were added to, respectively, \mathbf{K} and \mathbf{C} .

References

1. Åström KJ. Introduction to stochastic control theory: Courier Corporation; 2012.
2. Forbes PA, Chen A, Blouin J-S. Sensorimotor control of standing balance. *Handbook of clinical neurology*. 2018;159:61-83.
3. Proske U, Gandevia SC. The proprioceptive senses: their roles in signaling body shape, body position and movement, and muscle force. *Physiological reviews*. 2012.
4. Fitzpatrick R, Rogers DK, McCloskey D. Stable human standing with lower-limb muscle afferents providing the only sensory input. *The Journal of physiology*. 1994;480(2):395-403.
5. Mergner T, Schweigart G, Fennell L, Maurer C. Posture Control in Vestibular-Loss Patients. *Annals of the New York Academy of Sciences*. 2009;1164(1):206-15.
6. Young AS, Rosengren SM, Welgampola MS. Disorders of the inner-ear balance organs and their pathways. *Handbook of Clinical Neurology*. 2018;159:385-401.
7. Macefield VG, Knellwolf TP. Functional properties of human muscle spindles. *Journal of neurophysiology*. 2018;120(2):452-67.
8. Dimitriou M. Human muscle spindles are wired to function as controllable signal-processing devices. *Elife*. 2022;11:e78091.
9. Blum KP, Lamotte D'Incamps B, Zytnicki D, Ting LH. Force encoding in muscle spindles during stretch of passive muscle. *PLoS computational biology*. 2017;13(9):e1005767.
10. Proske U. What is the role of muscle receptors in proprioception? *Muscle & Nerve: Official Journal of the American Association of Electrodiagnostic Medicine*. 2005;31(6):780-7.
11. Kawato M. Internal models for motor control and trajectory planning. *Current opinion in neurobiology*. 1999;9(6):718-27.
12. Wolpert DM, Ghahramani Z, Jordan MI. An internal model for sensorimotor integration. *Science*. 1995;269(5232):1880-2.
13. Tedrake R. *Underactuated Robotics: Algorithms for Walking, Running, Swimming, Flying, and Manipulation (Course Notes for MIT 6.832)*. Downloaded on 20-08-2021 from <http://underactuated.mit.edu/>. 2021.
14. Wolpert DM. Computational approaches to motor control. *Trends in cognitive sciences*. 1997;1(6):209-16.
15. Scott SH. Optimal feedback control and the neural basis of volitional motor control. *Nature Reviews Neuroscience*. 2004;5(7):532-45.
16. Todorov E. Optimality principles in sensorimotor control. *Nature neuroscience*. 2004;7(9):907-15.

17. Slijkhuis FS, Keemink SW, Lanillos P. Closed-form control with spike coding networks. *IEEE Transactions on Cognitive and Developmental Systems*. 2023.
18. Boerlin M, Machens CK, Denève S. Predictive coding of dynamical variables in balanced spiking networks. *PLoS computational biology*. 2013;9(11):e1003258.
19. Calaim N, Dehmelt FA, Gonçalves PJ, Machens CK. The geometry of robustness in spiking neural networks. *Elife*. 2022;11:e73276.
20. Körding KP, Wolpert DM. Bayesian decision theory in sensorimotor control. *Trends in cognitive sciences*. 2006;10(7):319-26.
21. Peterka RJ. Sensory integration for human balance control. *Handbook of clinical neurology*. 2018;159:27-42.
22. Clemens IA, De Vrijer M, Selen LP, Van Gisbergen JA, Medendorp WP. Multisensory processing in spatial orientation: an inverse probabilistic approach. *Journal of Neuroscience*. 2011;31(14):5365-77.
23. Peterka RJ. Sensorimotor integration in human postural control. *Journal of neurophysiology*. 2002;88(3):1097-118.
24. Goodwin GM, McCloskey D, Matthews P. The contribution of muscle afferents to kinaesthesia shown by vibration induced illusions of movement and by the effects of paralysing joint afferents. *Brain*. 1972;95(4):705-48.
25. Hagbarth K-E, Vallbo Å. Discharge characteristics of human muscle afferents during muscle stretch and contraction. *Experimental Neurology*. 1968;22(4):674-94.
26. Edin BB, Vallbo A. Dynamic response of human muscle spindle afferents to stretch. *Journal of neurophysiology*. 1990;63(6):1297-306.
27. Edin BB, Vallbo A. Muscle afferent responses to isometric contractions and relaxations in humans. *Journal of neurophysiology*. 1990;63(6):1307-13.
28. Peters RM, Dalton BH, Blouin J-S, Inglis JT. Precise coding of ankle angle and velocity by human calf muscle spindles. *Neuroscience*. 2017;349:98-105.
29. Cordo PJ, Flores-Vieira C, Verschueren SM, Inglis JT, Gurfinkel V. Position sensitivity of human muscle spindles: single afferent and population representations. *Journal of neurophysiology*. 2002;87(3):1186-95.
30. Day J, Bent LR, Birznieks I, Macefield VG, Cresswell AG. Muscle spindles in human tibialis anterior encode muscle fascicle length changes. *Journal of Neurophysiology*. 2017;117(4):1489-98.
31. Kakuda N. Response of human muscle spindle afferents to sinusoidal stretching with a wide range of amplitudes. *The Journal of Physiology*. 2000;527(2):397-404.
32. Hulliger M, Nordh E, Vallbo A. The absence of position response in spindle afferent units from human finger muscles during accurate position holding. *The Journal of Physiology*. 1982;322(1):167-79.

33. Hulliger M, Nordh E, Vallbo A. Discharge in muscle spindle afferents related to direction of slow precision movements in man. *The Journal of Physiology*. 1985;362(1):437-53.
34. Dimitriou M, Edin BB. Discharges in human muscle spindle afferents during a key-pressing task. *The Journal of physiology*. 2008;586(22):5455-70.
35. Dimitriou M, Edin BB. Discharges in human muscle receptor afferents during block grasping. *Journal of Neuroscience*. 2008;28(48):12632-42.
36. Malik P, Jabakhanji N, Jones KE. An assessment of six muscle spindle models for predicting sensory information during human wrist movements. *Frontiers in computational neuroscience*. 2016;9:154.
37. Dimitriou M. Human muscle spindle sensitivity reflects the balance of activity between antagonistic muscles. *Journal of Neuroscience*. 2014;34(41):13644-55.
38. Dimitriou M, Edin BB. Human muscle spindles act as forward sensory models. *Current Biology*. 2010;20(19):1763-7.
39. Morasso PG, Sanguineti V. Ankle muscle stiffness alone cannot stabilize balance during quiet standing. *Journal of neurophysiology*. 2002;88(4):2157-62.
40. Morasso PG, Schieppati M. Can muscle stiffness alone stabilize upright standing? *Journal of neurophysiology*. 1999;82(3):1622-6.
41. Loram ID, Lakie M. Direct measurement of human ankle stiffness during quiet standing: the intrinsic mechanical stiffness is insufficient for stability. *The journal of physiology*. 2002;545(3):1041-53.
42. Casadio M, Morasso PG, Sanguineti V. Direct measurement of ankle stiffness during quiet standing: implications for control modelling and clinical application. *Gait & posture*. 2005;21(4):410-24.
43. Lockhart DB, Ting LH. Optimal sensorimotor transformations for balance. *Nature neuroscience*. 2007;10(10):1329-36.
44. Welch TD, Ting LH. A feedback model explains the differential scaling of human postural responses to perturbation acceleration and velocity. *Journal of neurophysiology*. 2009;101(6):3294-309.
45. Safavynia SA, Ting LH. Long-latency muscle activity reflects continuous, delayed sensorimotor feedback of task-level and not joint-level error. *Journal of neurophysiology*. 2013;110(6):1278-90.
46. Vallbo A. Human muscle spindle discharge during isometric voluntary contractions. Amplitude relations between spindle frequency and torque. *Acta Physiologica Scandinavica*. 1974;90(2):319-36.
47. Burke D, Hagbarth K-E, Löfstedt L. Muscle spindle responses in man to changes in load during accurate position maintenance. *The Journal of Physiology*. 1978;276(1):159-64.
48. Burke D, Hagbarth K-E, Löfstedt L. Muscle spindle activity in man during shortening and lengthening contractions. *The Journal of physiology*. 1978;277(1):131-42.

49. Miall RC, Wolpert DM. Forward models for physiological motor control. *Neural networks*. 1996;9(8):1265-79.
50. Brunton SL, Kutz JN. *Data-driven science and engineering: Machine learning, dynamical systems, and control*: Cambridge University Press; 2019.
51. Vette AH, Masani K, Nakazawa K, Popovic MR. Neural-mechanical feedback control scheme generates physiological ankle torque fluctuation during quiet stance. *IEEE Transactions on Neural Systems and Rehabilitation Engineering*. 2010;18(1):86-95.
52. Soames R, Atha J. The spectral characteristics of postural sway behaviour. *European journal of applied physiology and occupational physiology*. 1982;49:169-77.
53. Dong O, Graham C, Grewal A, Parrucci C, Ruina A. The bricycle: a bicycle in zero gravity can be balanced or steered but not both. *Vehicle system dynamics*. 2014;52(12):1681-94.
54. Meijaard JP, Papadopoulos JM, Ruina A, Schwab AL, editors. *Linearized dynamics equations for the balance and steer of a bicycle: a benchmark and review*. *Proceedings of the Royal Society of London A: Mathematical, Physical and Engineering Sciences*; 2007: The Royal Society.
55. Kooijman J, Meijaard JP, Papadopoulos JM, Ruina A, Schwab A. A bicycle can be self-stable without gyroscopic or caster effects. *Science*. 2011;332(6027):339-42.
56. Dong O, Graham C, Grewal A, Parrucci C, Ruina A. A bicycle in zero gravity is unrideable (The bricycle) 2014 [updated 17-03-2014]. Available from: <https://youtu.be/rNQdSfgJDNM?si=RXDK-mXVMDGpXtch>.
57. Maris E. A bicycle can be balanced by stochastic optimal feedback control but only with accurate speed estimates. *PLoS one*. 2023;18(2):e0278961.
58. Kiemel T, Oie KS, Jeka JJ. Multisensory fusion and the stochastic structure of postural sway. *Biological cybernetics*. 2002;87(4):262-77.
59. Jeka J, Kiemel T, Creath R, Horak F, Peterka R. Controlling human upright posture: velocity information is more accurate than position or acceleration. *Journal of neurophysiology*. 2004;92(4):2368-79.
60. Van Der Kooij H, De Vlugt E. Postural responses evoked by platform perturbations are dominated by continuous feedback. *Journal of neurophysiology*. 2007;98(2):730-43.
61. van der Kooij H, Jacobs R, Koopman B, Grootenboer H. A multisensory integration model of human stance control. *Biological cybernetics*. 1999;80:299-308.
62. Van Der Kooij H, Peterka RJ. Non-linear stimulus-response behavior of the human stance control system is predicted by optimization of a system with sensory and motor noise. *Journal of computational neuroscience*. 2011;30:759-78.

63. Kiemel T, Zhang Y, Jeka JJ. Identification of neural feedback for upright stance in humans: stabilization rather than sway minimization. *Journal of Neuroscience*. 2011;31(42):15144-53.
64. Campbell K, Lakie M. A cross-bridge mechanism can explain the thixotropic short-range elastic component of relaxed frog skeletal muscle. *The Journal of physiology*. 1998;510(3):941-62.
65. Campbell KS, Moss RL. A thixotropic effect in contracting rabbit psoas muscle: prior movement reduces the initial tension response to stretch. *The Journal of Physiology*. 2000;525(2):531-48.
66. Campbell KS, Moss RL. History-dependent mechanical properties of permeabilized rat soleus muscle fibers. *Biophysical journal*. 2002;82(2):929-43.
67. Blum KP, Campbell KS, Horslen BC, Nardelli P, Housley SN, Cope TC, et al. Diverse and complex muscle spindle afferent firing properties emerge from multiscale muscle mechanics. *Elife*. 2020;9:e55177.
68. Loram ID, Maganaris CN, Lakie M. Paradoxical muscle movement in human standing. *The Journal of physiology*. 2004;556(3):683-9.
69. Loram ID, Maganaris CN, Lakie M. Active, non-spring-like muscle movements in human postural sway: how might paradoxical changes in muscle length be produced? *The Journal of physiology*. 2005;564(1):281-93.
70. Loram ID, Maganaris CN, Lakie M. Human postural sway results from frequent, ballistic bias impulses by soleus and gastrocnemius. *The Journal of physiology*. 2005;564(1):295-311.
71. Di Giulio I, Maganaris CN, Baltzopoulos V, Loram ID. The proprioceptive and agonist roles of gastrocnemius, soleus and tibialis anterior muscles in maintaining human upright posture. *The Journal of physiology*. 2009;587(10):2399-416.
72. Kuo AD. An optimal state estimation model of sensory integration in human postural balance. *Journal of neural engineering*. 2005;2(3):S235.
73. Laurens J, Angelaki DE. A unified internal model theory to resolve the paradox of active versus passive self-motion sensation. *Elife*. 2017;6:e28074.
74. Crapse TB, Sommer MA. Corollary discharge across the animal kingdom. *Nature Reviews Neuroscience*. 2008;9(8):587-600.
75. Poulet JF, Hedwig B. New insights into corollary discharges mediated by identified neural pathways. *Trends in neurosciences*. 2007;30(1):14-21.
76. Angelaki DE, Cullen KE. Vestibular system: the many facets of a multimodal sense. *Annu Rev Neurosci*. 2008;31:125-50.
77. Laurens J, Angelaki DE. The functional significance of velocity storage and its dependence on gravity. *Experimental brain research*. 2011;210:407-22.
78. Jamali M, Carriot J, Chacron MJ, Cullen KE. Coding strategies in the otolith system differ for translational head motion vs. static orientation relative to gravity. *Elife*. 2019;8:e45573.

79. Fernandez C, Goldberg JM. Physiology of peripheral neurons innervating otolith organs of the squirrel monkey. II. Directional selectivity and force-response relations. *Journal of neurophysiology*. 1976;39(5):985-95.
80. Young E, Fernandez C, Goldberg J. Responses of squirrel monkey vestibular neurons to audio-frequency sound and head vibration. *Acta otolaryngologica*. 1977;84(1-6):352-60.
81. Angelaki DE, Yakusheva TA. How vestibular neurons solve the tilt/translation ambiguity: comparison of brainstem, cerebellum, and thalamus. *Annals of the New York Academy of Sciences*. 2009;1164(1):19-28.
82. Green AM, Angelaki DE. An integrative neural network for detecting inertial motion and head orientation. *Journal of neurophysiology*. 2004;92(2):905-25.
83. Green AM, Shaikh AG, Angelaki DE. Sensory vestibular contributions to constructing internal models of self-motion. *Journal of neural engineering*. 2005;2(3):S164.
84. Angelaki DE, McHenry MQ, Dickman JD, Newlands SD, Hess BJ. Computation of inertial motion: neural strategies to resolve ambiguous otolith information. *Journal of Neuroscience*. 1999;19(1):316-27.
85. Merfeld DM. Modeling the vestibulo-ocular reflex of the squirrel monkey during eccentric rotation and roll tilt. *Experimental Brain Research*. 1995;106(1):123-34.
86. Merfeld D, Zupan LH. Neural processing of gravito-inertial cues in humans. III. Modeling tilt and translation responses. *Journal of neurophysiology*. 2002;87(2):819-33.
87. Zupan LH, Merfeld DM, Darlot C. Using sensory weighting to model the influence of canal, otolith and visual cues on spatial orientation and eye movements. *Biological cybernetics*. 2002;86(3):209-30.
88. Roy JE, Cullen KE. Dissociating self-generated from passively applied head motion: neural mechanisms in the vestibular nuclei. *Journal of Neuroscience*. 2004;24(9):2102-11.
89. Brooks JX, Cullen KE. Early vestibular processing does not discriminate active from passive self-motion if there is a discrepancy between predicted and actual proprioceptive feedback. *Journal of neurophysiology*. 2014;111(12):2465-78.
90. Brooks JX, Carriot J, Cullen KE. Learning to expect the unexpected: rapid updating in primate cerebellum during voluntary self-motion. *Nature neuroscience*. 2015;18(9):1310-7.
91. DeCarlo RA. *Linear systems: A state variable approach with numerical implementation*: Prentice-Hall, Inc.; 1989.
92. Shampine LF, Reichelt MW. The matlab ode suite. *SIAM journal on scientific computing*. 1997;18(1):1-22.
93. Tremblay S. Height-to-Foot-Size Ratio [cited 2023 24-9]. Available from: <https://www.livestrong.com/article/491821-height-to-foot-size-ratio/>.

94. Rasman BG, Forbes PA, Peters RM, Ortiz O, Franks I, Inglis JT, et al. Learning to stand with unexpected sensorimotor delays. *Elife*. 2021;10:e65085.
95. Rajamani R. *Vehicle dynamics and control*: Springer Science & Business Media; 2011.
96. Bogdanov A. Optimal control of a double inverted pendulum on a cart. Oregon Health and Science University, Tech Rep CSE-04-006, OGI School of Science and Engineering, Beaverton, OR. 2004.
97. Dialynas G, Christoforidis C, Happee R, Schwab A. Rider control identification in cycling taking into account steering torque feedback and sensory delays. *Vehicle System Dynamics*. 2022:1-25.
98. A.L. Schwab JMP, A. Ruina and A. Dressel. JBike6, a benchmark for bicycle motion [cited 2022 14-7-2022]. Available from: http://ruina.tam.cornell.edu/research/topics/bicycle_mechanics/JBike6_web_folder.